universität wien

MASTERARBEIT | MASTER'S THESIS

Titel | Title

Operational Boundaries between Classical and Quantum Correlations

verfasst von | submitted by

Samuel Schlegel BSc

angestrebter akademischer Grad | in partial fulfilment of the requirements for the degree of

Master of Science (MSc)

Wien | Vienna, 2026

Studienkennzahl lt. Studienblatt | Degree programme code as it appears on the student record sheet:	UA 066 876
Studienrichtung lt. Studienblatt | Degree programme as it appears on the student record sheet:	Masterstudium Physics
Betreut von | Supervisor:	Assoz. Prof. Mag. Dr. Borivoje Dakic

Acknowledgements

I would like to express my sincere gratitude to my supervisor, Assoz. Prof. Mag. Dr. Borivoje Dakić, for his guidance, support, and for giving me the freedom to explore the questions that shaped this thesis. I am equally grateful to my co-supervisor, Dr. Flavio Del Santo, for many stimulating discussions, insightful feedback, and for consistently pushing for conceptual clarity.

I also thank Prof. Dr. Nicolas Gisin, Prof. Dr. Tomasz Paterek, and Dr. Ankit Kumar for inspiring conversations and insightful comments, as well as the colleagues and friends in Vienna whose questions, remarks, and informal exchanges helped refine many of the ideas presented here.

Finally, I thank my family and close friends, especially Mona, for their support throughout my studies. Any remaining errors are, of course, my own.

Abstract

Quantum features such as entanglement are often regarded as a sharp departure from classical physics. However, much of this view is due to the chosen representation, as many features that are regarded as benchmarks of allegedly quantum phenomena arise purely from the formalism, i.e., Hilbert space structures, rather than from the underlying genuinely quantum physical content. In this thesis we utilize the Wigner–Weyl formalism to formulate classical physics in a Hilbert space and quantum mechanics in a phase space language. This allows us to separate artifacts, which arise from the formalism, from the fundamental differences between quantum and classical physics.

After reviewing the phase space/Hilbert space correspondence and the Gaussian continuous–variable toolbox, we proceed to analyze how and when classical phase–space correlations can mimic quantum nonseparability when mapped to Hilbert space. We then introduce a hierarchy of boundaries to isolate the truly quantum signature. We separate quantum states from nonphysical Weyl–mapped operators by imposing a positivity constraint and further separate genuinely nonclassical resources that no longer admit a classical phase space description via Wigner–function negativity. This framework and the resulting boundaries motivate the notions of *representational entanglement* (covariance–based entanglement signal, despite operator negativity), *hybrid entanglement* (valid quantum entanglement within the classical–quantum overlap), and *genuine entanglement* beyond the overlap. As a consequence, we show that covariance–based witnesses can be misleading outside the Gaussian regime unless supplemented by explicit checks of nonclassicality and positivity.

Finally, we apply this approach to gravity–mediated entanglement proposals. We compare classical and quantum dynamics for typical initial states and identify where predictions of the two theories first diverge. The dynamical emergence of classical operator negativity suggests a dynamical route to representational entanglement and further clarifies what gravity–mediated entanglement tests can and cannot exclude.

Kurzfassung

Charakteristische quantenmechanische Phänomene wie die Verschränkung werden oft als starker Bruch mit der klassischen Physik angesehen. Viele dieser scheinbaren Besonderheiten kommen jedoch nicht durch die zugrunde liegende physikalische Theorie zustande, sondern durch die Art, wie sie mathematisch beschrieben werden. In dieser Arbeit benutzen wir den Wigner–Weyl Formalismus, um sowohl die klassische Physik in der Sprache der Quantenphysik auszudrücken, als auch der Quantenmechanik eine klassische Beschreibung zuzuschreiben. Das erlaubt es uns, Artefakte, die rein aus der gewählten Beschreibung entspringen, von den zugrundeliegenden robusten Unterschieden zu trennen.

Nach einer Darstellung der Dualität zwischen Phasenraum– und Hilbertraum–Beschreibung sowie einer Einführung in gaußsche kontinuierliche Variablen Systeme untersuchen wir, wie klassische Korrelationen im Phasenraum bei der Abbildung auf Operatoren scheinbare „Verschränkung“ erzeugen können. Daraus ergibt sich dann eine Hierarchie operativer Grenzen: Die Positivität des zugeordneten Operators trennt physikalisch zulässige Quantenzustände von nicht physikalischen, rein repräsentationsbedingten Artefakten. Innerhalb dieser positiven Zustände markiert die Negativität der Wigner–Funktion eine zweite Grenze zwischen klassisch reproduzierbaren und genuin nichtklassischen Zuständen. In diesem Kontext definieren wir repräsentative Verschränkung (Nichtseparierbarkeit trotz fehlender Positivität), hybride Verschränkung (echte Quantenkorrelationen, die jedoch klassisch imitiert werden können) und genuine Verschränkung jenseits dieses Bereichs. Ein zentrales Ergebnis ist, dass kovarianzbasierte (Verschränkungs–) Zeugen außerhalb des gaußschen Regimes ohne zusätzliche Positivitätsprüfungen irreführend sein können.

Abschließend werden wir dieses System auf zeitliche Entwicklung in Protokollen zur „gravitationsvermittelten Verschränkung“ anwenden und dabei klassische und quantenmechanische Dynamik vergleichen. Dabei wird sichtbar gemacht, ab welcher Ordnung der Potenzialentwicklung relevante Unterschiede auftreten, und wie das Auftreten von Negativität in der klassischen Hilbertraum–Evolution als dynamischer Ursprung repräsentativer Verschränkung interpretiert werden kann.

Contents

Acknowledgements i

Abstract iii

Kurzfassung v

1. Introduction 1

2. Phase Space / Hilbert Space Duality and Gaussian States 3

2.1. Classical Mechanics: Phase Space and Hilbert Space Representations 3

2.1.1. Classical Mechanics in Phase Space 4

2.1.2. Classical Mechanics in Hilbert Space 5

2.2. Quantum Mechanics: Hilbert Space and Phase Space Representations 8

2.2.1. Quantum Mechanics in Hilbert Space 8

2.2.2. Quantum Mechanics in Phase Space 10

2.3. Gaussian systems 12

2.3.1. Gaussian states and Gaussian unitaries 12

2.3.2. Separability and entanglement quantification 13

2.3.3. Non–classicality measures 14

3. Classical states in Hilbert space: correlations and nonseparability 17

3.1. Motivation and framework 17

3.1.1. Mapping and definitions 19

3.2. Gaussian systems: covariance criteria and their limitations 21

3.2.1. Classical Gaussian nonseparability 21

3.2.2. Beyond the Gaussian case: RS without positivity 25

3.3. Representational entanglement (RE): nonseparability without positivity 30

3.4. Hybrid entanglement (HE): entanglement in the classical–quantum overlap 34

3.5. Genuine entanglement (GE): positivity plus nonclassicality 38

3.6. Discussion 39

4. Time Evolution and Gravity-Mediated Entanglement: Classical vs. Quantum Dynamics **41**

4.1. Gravity–mediated entanglement: state of the art and literature . . . 41

4.2. The setup . . . 44

4.3. Evolution and covariance . . . 46

4.4. Results . . . 47

4.5. Discussion . . . 50

5. General Conclusion **53**

Bibliography **55**

A. Representational/Hybrid Entanglement **63**

A.1. Displaced mixtures in Hilbert space & numerical diagonalization . . . 63

A.2. Symplectic eigenvalue conditions . . . 66

A.3. Derivation of the kernel formula . . . 68

A.4. Hybrid beamsplitter state . . . 69

B. Gravity–Mediated Entanglement **71**

B.1. GME setup and evolution . . . 71

B.2. Numerical details . . . 75

B.2.1. Parameters . . . 75

B.2.2. Robertson–Schrödinger condition . . . 75

B.2.3. Wigner function . . . 76

1. Introduction

According to the standard narrative, quantum mechanics shattered our classical and intuitive picture of reality: superposition, entanglement, indeterminism, contextuality, and nonlocality are thought to be genuinely quantum. However, much of this narrative blends together the mathematical framework used to describe a theory, with the physical content that distinguishes that theory. In particular, if one allows classical theories to be fundamentally indeterministic, many paradoxes, but also features that are typically attributed to quantum mechanics, obtain classical analogues. In a recent work, this point has been made explicit by showing classical variants of the measurement problem, single particle non-locality, classical no-cloning, and even forms of classical "entanglement". This can be recovered in suitably indeterministic classical models, while what remains genuinely non–classical is the existence of incompatible physical variables tied to a non–zero value of Planck's reduced constant $\hbar$ [1].

This thesis sets out from that perspective. Rather than beginning with the familiar dichotomy "classical = phase space, quantum = Hilbert space" and accepting that the formalisms themselves define the physics, we take a comparative route instead. We present both classical and quantum theories in each other's language, i.e., classical mechanics in a Hilbert space guise and quantum mechanics in phase space. This approach allows us to ask a sharper question: which features are artifacts of the formalism and which are fundamental physical differences between classical and quantum physics?

The practical motivation is twofold. Foundationally, mapping the two theories into a common language clarifies where and why they differ: incompatibility of observables (and the $\hbar$-dependent uncertainty relations that follow) is a structural feature of quantum theory that cannot be reproduced by any classical theory lacking incompatible variables. In practice, phase space and Hilbert space cross representations are often used in semi–classical approximations and quantum information tasks. Understanding their limits helps to import intuition and techniques across domains.

Historically, this perspective also helps nuance textbook narratives. For instance, many early arguments "proving" the necessity of quantized [2] can be re-examined through the lens of semi-classical models. For instance, treating matter quantum-mechanically but the electromagnetic field classically can reproduce many features of the photoelectric effect, which was first considered by Lamb & Scully [3]. It was

only later that the need to quantize the field in full generality became compelling and necessary. The experimental program that began with the Freedman and Clauser's Bell-inequality tests in the 1970s played a decisive role in separating quantum predictions from a broad class of classical alternatives [4].

This thesis is organized as follows: Chapter 2 lays out the two mathematical formalisms, the phase space formulation and the Hilbert space formulation, and shows precisely how one may map objects from one description to the other via the Wigner-Weyl transform. Chapter 3, based on our work in Ref. [5], discusses how classically correlated phase space distributions can violate entanglement criteria for quantum states. Finally, we apply the framework developed here to contemporary gravity–mediated entanglement proposals.

By separating the representational aspects from the fundamental ones, the goal of this work is to reduce conceptual confusion and to provide a clearer map of where classical intuition can safely be used, and where quantum theory demands genuinely new concepts.

2. Phase Space / Hilbert Space Duality and Gaussian States

This chapter develops two complementary mathematical pictures that will be used throughout the thesis. The *phase space* picture, where states are distributions on coordinates (q, p), and the *Hilbert space* picture, where states are vectors on operators acting on a complex Hilbert space. As mentioned in the introduction, the motivation is both conceptual and practical, as many concepts usually labeled as "quantum" are intertwined with the choice of formalism. By casting classical and quantum theories in the same mathematical language, we can separate what is truly physical from what is a byproduct of representation.

Below we first present classical mechanics in both phase space (Sec. 2.1.1) and a Hilbert space representation (Sec. 2.1.2). We then review the standard Hilbert space picture of quantum mechanics (Sec. 2.2.1) and its phase space counterpart (Sec. 2.2.2). Finally, Gaussian systems and their properties (e.g., separability) will be discussed (Sec. 2.3). All of these correspondences will finally be collected in Table 1. This dual presentation prepares more systematic comparisons from Chapter 3 onward.

2.1. Classical Mechanics: Phase Space and Hilbert Space Representations

Classical mechanics is most commonly formulated in phase space, where states are represented by probability distributions $\rho(q, p, t)$, and their dynamics are governed by the Liouville equation, with Poisson brackets determining the evolution of observables. At the same time, this is not the only possible representation. One can equivalently reformulate classical mechanics in a Hilbert space language, where classical states are encoded in L^2–type objects and evolve unitarily under an appropriate generator. This alternative representation is particularly useful for structural comparisons with quantum theory and will provide the bridge to the Wigner–Weyl framework developed below.

2.1.1. Classical Mechanics in Phase Space

A classical state for a system with n degrees of freedom is most generally represented in phase space $\Gamma \cong \mathbb{R}^{2n}$, where states take the form of a probability distribution $\rho(q,p,t)$. Pure phase space states are represented by Dirac deltas $\rho(q,p) = \delta(q - q_0)\delta(p - p_0)$, while statistical ensembles and incomplete knowledge are described by well–behaved probability densities (mixed states). Observables are then real-valued functions $f(q,p)$ on Γ, and expectation values are computed as $\langle f \rangle = \int f(q,p)\rho(q,p,t)\, dq\, dp$.

It is convenient to derive the phase space picture from the Lagrangian $L(q,\dot{q},t)$ via the Legendre transform

$$p_i \;=\; \frac{\partial L}{\partial \dot{q}_i}, \qquad H(q,p,t) = \sum_i \dot{q}_i p_i - L(q,\dot{q},t), \tag{2.1}$$

which yields Hamilton's equations

$$\dot{q}_i = \frac{\partial H}{\partial p_i}, \qquad \dot{p}_i = -\frac{\partial H}{\partial q_i}. \tag{2.2}$$

For an ensemble described by $\rho(q,p,t)$ the dynamics are governed by the Liouville equation

$$\frac{\partial \rho}{\partial t} + \{\rho, H\} = 0, \tag{2.3}$$

where $\{\cdot,\cdot\}$ defines the Poisson bracket

$$\{f,g\} = \sum_{i=1}^{n} \Big(\frac{\partial f}{\partial q_i}\frac{\partial g}{\partial p_i} - \frac{\partial f}{\partial p_i}\frac{\partial g}{\partial q_i} \Big). \tag{2.4}$$

The Poisson bracket gives the algebra of phase space functions a Lie algebra structure and the fundamental Poisson brackets for the canonical variables themselves are

$$\{q_i, q_j\} = 0, \tag{2.5}$$
$$\{p_i, p_j\} = 0, \tag{2.6}$$
$$\{q_i, p_j\} = \delta_{ij}. \tag{2.7}$$

A key feature of the Poisson brackets is that they are invariant under canonical transformations. This means that any expressions that are built from the Poisson brackets retain their form regardless of the canonical coordinates chosen. This is particularly useful if we consider the equation of motion for a function $u(q,p,t)$, which can be written as

$$\frac{du}{dt} = \{u, \mathcal{H}\} + \frac{\partial u}{\partial t}, \tag{2.8}$$

where we can immediately see that Hamilton's equations are simply special cases of the above equation [6]

$$\dot{q}_i = \{q_i, \mathcal{H}\}, \tag{2.9}$$
$$\dot{p}_i = \{p_i, \mathcal{H}\}. \tag{2.10}$$

Finally, to shorten the evolution equation, the Liouville operator [7]

$$\mathcal{L} = i\{\mathcal{H}, \cdot\} = i\sum_j \frac{\partial \mathcal{H}}{\partial q^j}\frac{\partial}{\partial p_j} - i\frac{\partial \mathcal{H}}{\partial p_j}, \frac{\partial}{\partial q^j} \tag{2.11}$$

is introduced to write the evolution of $\rho(x, p, t)$ in a more compact form

$$i\dot{\rho} = \mathcal{L}\rho. \tag{2.12}$$

2.1.2. Classical Mechanics in Hilbert Space

A first Hilbert space reformulation of classical mechanics is the Koopman–von Neumann (KvN) formalism. In KvN, one introduces complex amplitudes on phase space, $\psi(q, p, t) \in L^2(\Gamma)$, whose evolution is unitary and generated by the Liouville operator. In this way, classical Liouville dynamics is written in a Hilbert space language while preserving classical predictions for phase space densities. We will not adopt KvN as our main framework, because its wavefunctions live in an auxiliary Hilbert space and do not represent physical quantum states, which makes the physical interpretation less transparent for the present comparison [8].

Instead, we use the Wigner–Weyl (WW) framework. WW sets up a correspondence between phase space functions and Hilbert space operators, so that classical and quantum descriptions can be written in closely parallel mathematical forms. This makes it particularly suitable for our purposes, because by starting from the classical phase space product, one can introduce a deformed (non-commutative) product that reproduces quantum operator composition. In other words, WW provides a controlled route from classical phase space algebra to the quantum one, which is precisely the bridge needed in the following sections [9].

The WW approach dates back to Hermann Weyl's 1927 paper [10], which sought a systematic way to "quantize" classical functions by treating position and momentum on entirely symmetric footing. For a sufficiently well-behaved phase space function $f(q, p)$, the Weyl quantization map Φ is defined by

$$\Phi[f] \equiv \hat{f} \;=\; \int_{\mathbb{R}^{2n}} da\, db\, \tilde{f}(a, b)\, e^{\frac{i}{\hbar}(a\cdot\hat{q}+b\cdot\hat{p})}, \tag{2.13}$$

where the Fourier transform $\tilde{f}(a, b)$ is

$$\tilde{f}(a, b) \;=\; \frac{1}{(2\pi\hbar)^n}\int_{\mathbb{R}^{2n}} dq\, dp\; f(q, p)\, e^{-\frac{i}{\hbar}(a\cdot q+b\cdot p)}. \tag{2.14}$$

Here a, b are integration variables, and the normalization factor $(2\pi\hbar)^{-n}$ ensures Φ maps the constant function 1 to the identity operator $\mathbb{I}$. Additionally, for polynomial functions, the Weyl map yields the completely symmetrized operator ordering, e.g., $\Phi[qp] = (\hat{q}\hat{p} + \hat{p}\hat{q})/2$ [9].

It is important to note that the Weyl quantization procedure cannot yet serve as a fully consistent quantization map [11]. The argument for this was first proposed in 1946 by Groenewold [12] and goes as follows: A quantization map Q with

$$Q : C^\infty(\mathbb{R}^{2n}) \longrightarrow \{\text{operator on a Hilbert space}\}, \tag{2.15}$$

needs to satisfy

1. Normalization: $Q(1) = \mathbb{I}$,

2. Canonical variables: $Q(q_i) = \hat{q}_i, Q(p_i) = \hat{p}_i$,

3. Dirac condition:
$$Q(\{f, g\}) = \frac{1}{i\hbar}[Q(f), Q(g)], \tag{2.16}$$

i.e., Poisson brackets mapping to commutators. Groenewold showed that no quantization map can satisfy all of the above conditions on the full Poisson algebra. In particular, one finds a failure of the Dirac condition in WW formalism at the cubic order [11]
$$i\hbar Q(\{q^2p, qp^2\}) \neq [Q(q^2p), Q(qp^2)]. \tag{2.17}$$

The theorem proves that *no quantization map* can preserve the Poisson algebra exactly. Consequently, classical mechanics cannot be "quantized" by merely replacing Poisson brackets with commutators—a foundational insight of the *Groenewold-van Hove theorem* [11–13]. To obtain the quantum-level operator correspondence, the classical phase space product must therefore be replaced by an appropriate non-commutative product (defined below).

For the Weyl quantization map $\Phi[f]$, this implies that it fails to satisfy

$$[\Phi[f], \Phi[g]] = i\hbar\Phi(\{f, g\}) \tag{2.18}$$

exactly for all f, g. To restore this property, the requirement that Poisson brackets map exactly to operator commutators (i.e., property (3.)) has to be relaxed. We have to replace the regular multiplication and the Poisson bracket in phase space with the Moyal $\star$–product and the corresponding bracket. This deforms the classical

algebra, such that the Weyl map is upgraded to an exact algebra isomorphism. This $\star$–product is given by

$$f \star g = f(q,p) \exp\left[\frac{i\hbar}{2}(\overleftarrow{\partial_q}\overrightarrow{\partial_p} - \overleftarrow{\partial_p}\overrightarrow{\partial_q})\right] g(q,p), \tag{2.19}$$

where $\overleftarrow{\partial}$ and $\overrightarrow{\partial}$ denote derivatives acting to the left and to the right, respectively. The expansion can be rewritten in orders of $\hbar$ via

$$f \star g = fg + \frac{i\hbar}{2}\{f,g\} - \frac{\hbar^2}{8}\{\{f,g\}\} + \mathcal{O}(\hbar^3), \tag{2.20}$$

where $\{\{f,g\}\}$ denotes the second order differential operator of the exponential expansion. Now the kinematic relation under the $\star$-product is known as the *Moyal bracket*

$$\{f,g\}_{\mathrm{MB}} = \frac{1}{i\hbar}(f \star g - g \star f) \tag{2.21}$$

and satisfies

$$\{f,g\}_{\mathrm{MB}} = \{f,g\} + \mathcal{O}(\hbar^2) \tag{2.22}$$

by construction. We can therefore view classical mechanics itself as governed by a deformed noncommutative algebra, where the deformation parameter is $\hbar$. Note that this bracket obeys the full Jacobi identity and makes $(C^\infty, \star)$ a genuine associative algebra [14].

Using both the Moyal product and the Moyal bracket, the Weyl quantization map $\Phi : f \to \hat{f}$ becomes an exact algebra homomorphism, satisfying

$$\Phi[f \star g] = \Phi[f]\Phi[g], \quad \Phi(\{f,g\}_{\mathrm{MB}}) = \frac{1}{i\hbar}[\Phi[f], \Phi[g]], \tag{2.23}$$

and therefore bypassing the Groenewold-van Hove obstruction.

Because the Moyal bracket satisfies the Jacobi identity exactly, it restores closure of the algebra and lets us treat classical observables as though they form a noncommutative quantum algebra.

This can be used to get a classical von Neumann equation 2.31 by Weyl transforming eq. 2.12 in matrix elements $\rho(x,y,t) = \langle x| \hat{\rho}(t) |y\rangle$, first derived by Bohm and Hiley [7]

$$i\hbar\frac{\partial}{\partial t}\rho(x,y,t) = -\frac{\hbar^2}{2m}\left(\frac{\partial}{\partial x^2} - \frac{\partial}{\partial y^2}\right)\rho(x,y,t) + (x-y)V'\left(\frac{x+y}{2}\right)\rho(x,y,t). \tag{2.24}$$

In this thesis, we will exploit this exact isomorphism, as well as the classical von Neumann equation (CvN), to examine classical analogues of entanglement, as well as its implications on current gravity–mediated entanglement proposals.

2.2. Quantum Mechanics: Hilbert Space and Phase Space Representations

Quantum theory is most commonly expressed in the *Hilbert space formulation*, where pure states are rays $|\psi\rangle$ and mixed states are represented by density operators ρ, while observables are self–adjoint operators (Sec. 2.2.1). Yet it admits an entirely one–to–one *phase space formulation* (Sec. 2.2.2), in which the Wigner function and Wigner–transformed operators encode states and operators as functions on the phase space, with the Moyal $\star$-product replacing operator multiplication.

2.2.1. Quantum Mechanics in Hilbert Space

Quantum states are represented, in general, by density operators ρ on a complex Hilbert space $\mathscr{H}$: $\rho \geq 0$ and $\operatorname{Tr}\rho = 1$ [15]. This is directly analogous to classical mechanics, where states are probability distributions and pure states are a special subset (delta distributions). In quantum mechanics, pure states are the extremal density operators, equivalently rank-one projectors $\rho = |\psi\rangle\langle\psi|$ (with $|\psi\rangle$ defined up to a global phase, i.e., rays), while mixed states are convex combinations

$$\rho = \sum_i \omega_i |\psi_i\rangle\langle\psi_i|, \qquad \omega_i \geq 0, \ \sum_i \omega_i = 1. \tag{2.25}$$

Thus, mixed states describe statistical uncertainty (or reduced states of entangled composites), and pure states arise as the special case with no mixing. For example, for a spin-$\frac{1}{2}$ system,

$$\rho = \tfrac{1}{2}(|\uparrow\rangle\langle\uparrow| + |\downarrow\rangle\langle\downarrow|) \tag{2.26}$$

is maximally mixed ($S(\rho) = \ln 2$), whereas any pure state projector has $S(\rho) = 0$ [16].

Observables are typically represented by Hermitian operators $A : \mathscr{H} \to \mathscr{H}$. The spectral theorem always allows the following decomposition for discrete/continuous operators

$$A = \sum_k \lambda_k E_k \quad \text{or} \quad A = \int \lambda dE(\lambda), \tag{2.27}$$

where the set $\{E_k\}$ and $E(\lambda)$ are orthogonal projectors onto the eigen-subspaces of the operator [15]. Physical expectation values in the state ρ are then calculated via $\langle A\rangle = \operatorname{Tr}[\rho A]$ for mixed states, while the expression reduces to $\langle\psi| A |\psi\rangle$ for pure states.

The dynamics of quantum mechanics is governed by the time–dependent Schrödinger equation

$$i\hbar\frac{d}{dt}|\psi(t)\rangle = \mathcal{H}|\psi(t)\rangle \tag{2.28}$$

and can be solved via the time evolution operator $U(t)$

$$|\psi(t)\rangle = U(t)\,|\psi(0)\rangle\,, \quad \text{with} \quad U(t) = \exp(-\frac{i}{\hbar}\mathcal{H}t) \tag{2.29}$$

in the Schrödinger picture. A completely equivalent formulation is also possible in the Heisenberg picture, where the operators carry the time dependence [17]

$$A_H(t) = U^\dagger(t)AU(t), \quad i\hbar\frac{dA_H(t)}{dt} = [A_H, \mathcal{H}]. \tag{2.30}$$

Of particular interest to us is the von Neumann equation

$$i\hbar\frac{d\rho}{dt} = [\mathcal{H}, \rho]. \tag{2.31}$$

Furthermore, for discrete observables, like in Eq. (2.27), the Born rule assigns probabilities for a measurement outcome $\Pr(\lambda_k) = \mathrm{Tr}[\rho E_k]$ to a system that is in the state ρ. The post–measurement update rule (Lüders rule) for a projective measurement with an outcome λ_k is given by [18]

$$\rho \mapsto \frac{E_k \rho E_k}{\mathrm{Tr}[\rho E_k]}. \tag{2.32}$$

More generally, measurement processes are modeled by POVMs $\{F_m\}$ with $F_m \geq 0$ and $\sum_m F_m = I$, and the set of possible state updates depends on the specific instrument used. Note that the Born rule (a probability rule) is logically distinct from a collapse/update rule [19]; interpretations of quantum theory differ on whether and how a collapse occurs [20]. For bipartite systems, pure joint states can give mixed reduced states, e.g., a pure entangled state $|\Psi\rangle_{AB}$ can induce a mixed reduced density $\rho_A = \mathrm{Tr}_B[|\Psi\rangle\langle\Psi|]$, a fact that motivates careful distinctions between ensemble mixtures and reduced-state mixtures when discussing uncertainty and information.

To treat quantum correlations, we can compose our Hilbert space of two subsystems $\mathscr{H}_A$, $\mathscr{H}_B$ via the tensor product $\mathscr{H}_{AB} = \mathscr{H}_A \otimes \mathscr{H}_B$. Separable states can then be decomposed as $\rho_A \otimes \rho_B$, while states that cannot be written in this manner are called *entangled*. To quantify entanglement, many criteria/witnesses can be used for bipartite systems. For instance, entanglement entropy $S(\rho_A) = -\mathrm{Tr}[\rho_A \ln \rho_A]$ is a very versatile criterion, but might be challenging to compute [21]. In practice, computable criteria are often preferred. In particular, we will use PPT- and covariance-based tests in Sec. 2.3 below.

2.2.2. Quantum Mechanics in Phase Space

The Wigner–Weyl formalism also embeds quantum mechanics into phase space through the inverse of the Weyl map introduced in Sec. 2.1.2, namely the *Wigner transform*. The Wigner function of a pure state $|\psi\rangle$ is given by [22, 23]

$$W(q,p) = \frac{1}{2\pi\hbar}\int_{-\infty}^{\infty} dy e^{-\frac{i}{\hbar}py}\psi\left(q+\frac{y}{2}\right)\psi^*\left(q-\frac{y}{2}\right), \tag{2.33}$$

where the marginals can be obtained by integrating out one quadrature

$$\int W dp = |\psi(q)|^2, \quad \int W dq = |\tilde{\psi}(p)|^2. \tag{2.34}$$

This phase space function is real–valued, but it can take negative values [24]. Naturally, this formalism can be extended to cover quantum systems described by a density operator ρ in $L^2(\mathbb{R})$ via

$$W(q,p) = \frac{1}{2\pi\hbar}\int_{-\infty}^{\infty} dy e^{-\frac{i}{\hbar}py}\left\langle q+\frac{y}{2}\right|\rho\left|q-\frac{y}{2}\right\rangle. \tag{2.35}$$

By construction, for a normalized density operator, W is real and normalized. Moreover, its marginal distributions reproduce the known position and momentum probabilities

$$\int_{-\infty}^{\infty} W(q,p)dp = \langle q|\rho|q\rangle, \quad \int_{-\infty}^{\infty} W(q,p)dq = \langle p|\rho|p\rangle. \tag{2.36}$$

Again, despite being real and normalized, W may take negative values, a hallmark of nonclassical features, and are therefore called *quasiprobabilities* [23].
To move beyond state-only representations, the operators $\hat{A}$ on $\mathscr{H}$ have to be mapped to functions on phase space as well. Taking Eq. 2.35 and applying it to $\hat{A}$ yields

$$A_W(q,p) = \frac{1}{2\pi\hbar}\int_{-\infty}^{\infty} dy e^{-\frac{i}{\hbar}py}\left\langle q+\frac{y}{2}\right|\hat{A}\left|q-\frac{y}{2}\right\rangle. \tag{2.37}$$

This map is one-to-one and is properly normalized. The identity operator $\mathbb{I}$ is mapped to 1, and the projectors $|q_0\rangle\langle q_0|$ and $|p_0\rangle\langle p_0|$ are mapped to the delta-distributions $\delta(q-q_0)$ and $\delta(p-p_0)$ respectively. Importantly, these operators and their corresponding symbols satisfy the trace relation

$$\mathrm{Tr}[\hat{A}\hat{B}] = \iint A_W(q,p)B_W(q,p)dqdp. \tag{2.38}$$

Lastly, these Wigner–transformed operators correspond to a *completely symmetrized* operator ordering

$$(q^n p^m)_W \to \frac{1}{2^n}\sum_{r=0}^{n}\binom{n}{r}\hat{q}^{n-r}\hat{p}^m\hat{q}^r, \tag{2.39}$$

thus eliminating ambiguity at each order [25].

To connect the algebra of operators with their phase space counterparts, the Moyal product from eq. 2.21 is used. In particular, the Moyal product is required to generalize the standard expectation value

$$\langle \hat{A} \rangle = \mathrm{Tr}[\hat{\rho}\hat{A}] = \iint A_W(q,p) W(q,p) dq dp, \tag{2.40}$$

to higher–order correlations, such as

$$\langle \hat{A}\hat{B} \rangle = \iint A_W \star B_W W dq dp, \tag{2.41}$$

encoding interference through the $\star$–product [26]. Negative regions (see Sec. 2.3.3) in W and non-Poissonian $\star$–commutators of phase space operators, serve as diagnostics for squeezing, quantum entanglement, and contextuality [27]. Lastly, the Moyal bracket is used to generate the quantum Liouville equation in phase space

$$\frac{\partial W}{\partial t} = \{\mathcal{H}, W\}_{\mathrm{MB}}. \tag{2.42}$$

This quantum phase space evolution is central to a broad class of practical semiclassical and mixed quantum–classical schemes, because it provides a controlled route to approximations obtained by expanding the $\hbar$-dependent quantum corrections around the classical Poisson bracket and retaining only leading terms (e.g., linearized/classical–Wigner or truncated–Wigner dynamics). Such truncations underpin widely used semiclassical phase space methods and their systematic analyses [26], and they form the computational basis of several approaches in chemical physics for time-correlation functions, spectroscopy, and molecular dynamics [28–30]. More generally, extensions to open-system dynamics can be incorporated in this framework through suitable dissipative and noise terms, providing a phase space description of decoherence processes [31]. This flexibility will be relevant later when discussing gravity-mediated entanglement scenarios. In conclusion, the phase space formulation of quantum mechanics thus provides both an intuitive visualization of quantum phenomena and a quantitative approach to semi–classical approximations, state reconstruction [32] and the study of the dynamics of open systems.

A side-by-side summary of the classical/quantum correspondences across phase space and Hilbert space formalisms is given in Table 1.

Table 1.: Comparison of states, evolution, kinematics, measurement, and entanglement in classical and quantum mechanics, across Hilbert and phase space formalisms.

	Phase space		**Hilbert space**	
	Classical	**Quantum**	**Classical**	**Quantum**
State	$f(q,p) \geq 0$	$W(q,p)$ may be negative	$\hat{\rho}_f$ need not be positive	$\hat{\rho} \geq 0$
Evolution	$\partial_t f = \{H, f\}_{\mathrm{PB}}$	$\partial_t W = \{H, W\}_{\mathrm{MB}}$	CvN	von Neumann
Kinematics	$\{q,p\}_{\mathrm{PB}} = 1$	$\{\cdot,\cdot\}_{\mathrm{MB}} = \{\cdot,\cdot\}_{\mathrm{PB}} + O(\hbar^2)$	$[\hat{q},\hat{p}] = i\hbar$	$[\hat{q},\hat{p}] = i\hbar$
Measurement	conditioning Bayes update	projectors $\mapsto \delta$ POVMs $\mapsto$ overlaps	formal $\mathrm{Tr}[\hat{\rho}_f M]$ not always positive	Born rule: projective/POVM
Entanglement	probabilistic correlations only	genuine entanglement (PPT/RS)	representational "entanglement" from non-positive $\hat{\rho}_f$	operational quantum entanglement

2.3. Gaussian systems

Gaussian systems are introduced here as the technical bridge to Chapter 3. For two-mode Gaussian states, second moments fully characterize the state, so covariance methods give closed-form and computable entanglement tests. This makes them the cleanest setting to separate three logically distinct questions: (i) kinematics of states and Gaussian evolutions (Sec. 2.3.1), (ii) separability tests based on partial transpose and a computable monotone (Sec. 2.3.2), and (iii) stronger non-classicality diagnostics beyond covariance data (Sec. 2.3.3). This distinction will be essential later, where covariance-based nonseparability can appear without genuine quantum non-classicality. Overviews of these methods are given in the literature [33–35].

2.3.1. Gaussian states and Gaussian unitaries

We now introduce continuous-variable quantum states of bosonic modes. For n modes, each mode is described by two canonical observables: a position-like quadrature q_j and a momentum-like quadrature p_j. A *Gaussian state* is a continuous-variable state whose Wigner function is Gaussian in phase space, or equivalently, it is completely characterized by the first and second moments of the quadratures.

The canonical quadratures q_j, p_j satisfy the commutation relation

$$[q_i, p_j] = i\hbar\delta_{ij} \tag{2.43}$$

and are collected in a vector (where the ordering is arbitrary, but will change the symplectic form)

$$R = (q_1, p_1, \ldots, q_n, p_n)^T. \tag{2.44}$$

The block diagonal symplectic form that will be used for the most part in this thesis is given by

$$\Omega = \bigoplus_{i=1}^{n} \begin{pmatrix} 0 & 1 \\ -1 & 0 \end{pmatrix} \tag{2.45}$$

and allows for the compact version of the uncertainty relation $[R_i, R_j] = i\hbar\Omega_{ij}$. Therefore, to specify any Gaussian fully, we require the vector of first moments $\bar{R}$ and the covariance matrix Σ defined as [36]

$$\Sigma_{ij} = \frac{1}{2}\langle R_i R_j + R_j R_i\rangle - \langle R_i\rangle\langle R_j\rangle, \tag{2.46}$$

$$\text{and} \quad \bar{R} = \langle R\rangle. \tag{2.47}$$

Note that for a quantum Gaussian state, the covariance matrix needs to satisfy the *Robertson-Schrödinger uncertainty relation* [33]

$$\Sigma + \frac{i\hbar}{2}\Omega \succeq 0, \tag{2.48}$$

in matrix form.

Now that Gaussian states are completely specified by $(\bar{R}, \Sigma)$, one may ask how they transform. *Gaussian unitaries* (which map Gaussian states to Gaussian states) are generated from a Hamiltonian $\mathcal{H}$, via $U = \exp(-i\mathcal{H}t/\hbar)$, where $\mathcal{H}$ is at most quadratic in q and p. These transformations are called symplectic transformations, $S \in Sp(2n, \mathbb{R})$ (i.e. $S\Omega S^T = \Omega$) and act on the first moments and on the first moments via

$$\Sigma \to S\Sigma S^T, \qquad \bar{R} \to S\bar{R} + d, \tag{2.49}$$

respectively [36]. Hence, in the Gaussian sector, dynamics and correlations can be tracked entirely at the level of $(\bar{R}, \Sigma)$, which is why covariance criteria become the natural first layer of analysis.

2.3.2. Separability and entanglement quantification

To see whether a Gaussian state is separable or to quantify its validity (in an uncertainty relation sense), the *symplectic eigenvalues* are required. They are mainly used for the Gaussian PPT criterion [33] and the logarithmic negativity [35].

Williamson's theorem states that every real, positive definite $2n \times 2n$ covariance matrix Σ can be decomposed as

$$\Sigma = S^T \mathrm{diag}(\nu_1, \nu_2 \ldots, \nu_n) S, \tag{2.50}$$

where $\nu_k > 0$ are the symplectic eigenvalues. The ν_k are physically meaningful, because entropic quantities are typically functions of $\{\nu_k\}$ [36]. To calculate these eigenvalues in practice, the matrix $i\Omega\Sigma$ is formed, and its pairs of eigenvalues $\{\pm i\nu_k\}$ are computed. The positive ν_k are then taken as the symplectic eigenvalues [37].

For bipartite (two-mode) Gaussian systems, the Peres–Horodecki (PPT) criterion has a covariance-matrix formulation that is necessary and sufficient for separability within this class [33,38]. In phase space, partial transposition is implemented by reflecting one momentum quadrature (e.g., $p_2 \to -p_2$) [33]. Defining

$$\Lambda_{\mathrm{PT}} = \mathrm{diag}(1, 1, 1, -1), \tag{2.51}$$

the partially transposed covariance matrix is

$$\Sigma^{\Gamma} = \Lambda_{\mathrm{PT}} \Sigma \Lambda_{\mathrm{PT}}. \tag{2.52}$$

The *Gaussian PPT criterion* then demands that Σ^{Γ} must still represent a physical covariance matrix, i.e.

$$\Sigma^{\Gamma} + \frac{i\hbar}{2}\Omega \succeq 0. \tag{2.53}$$

Equivalently, if $\{\tilde{\nu}_k\}$ are the symplectic eigenvalues of Σ^{Γ}, with smallest one $\tilde{\nu}_-$, separability is equivalent to

$$\tilde{\nu}_- \geq \hbar/2, \tag{2.54}$$

while $\tilde{\nu}_- < \hbar/2$ signals entanglement (PPT violation) [33].

Logarithmic negativity E_N is a computable entanglement monotone. In terms of $\tilde{\nu}_-$,

$$E_N = \max\{0, -\ln(2\tilde{\nu}_-/\hbar)\}, \tag{2.55}$$

so the covariance formalism directly provides both a separability test and a quantitative entanglement measure for bipartite Gaussian states [35,36].

2.3.3. Non–classicality measures

While the covariance/PPT tests above test direct correlations and Gaussian entanglement, genuine non-classicality usually requires negativity of the phase space quasi–probabilities. The two main ways to check this are either via the negativity (volume) of the *Wigner function* or by checking the behavior of the *Glauber–Sudarshan P-function*, i.e. the diagonal coherent-state representation

$$\rho = \int d^2\alpha \, P(\alpha) \, |\alpha\rangle\langle\alpha|, \tag{2.56}$$

which plays the role of a phase space distribution over coherent states [39,40].

The Wigner function of a quantum state $W(q,p)$ (Sec. 2.2.2) may take negative values, which can be measured by the negativity volume

$$\delta(W) = \left(\iint |W(q,p)| dqdp - 1 \right), \tag{2.57}$$

where $\delta(W) > 0$ is a clear non–classical signature that cannot arise from any well behaved positive classical phase space distribution [41].

Another possible criterion is given by the non–positivity (or highly singular behavior) of the P–function. This is a stronger criterion that says that if the P–function is not a genuine probability distribution, we are unable to depict the state as a mixture of coherent states and therefore cannot assign it a classical description [25,42].

Note that a Gaussian Wigner function may be strictly positive, but the state is non-classical in other senses (e.g., violating the uncertainty relation). Also note that non–Gaussian operation will typically lead to an emergence of Wigner–negativity in many scenarios. This is the link that we will exploit when looking at genuine quantum entanglement in Sec. 3.5.

3. Classical states in Hilbert space: correlations and nonseparability

This chapter asks a pragmatic question: what do correlation witnesses actually certify when classical statistics are analyzed with Hilbert space tools?

The central message is that "entanglement-like" signatures appear at different levels, depending on prior assumptions and on what is operationally accessible to a (possibly restricted) observer. Some signatures are purely *representational* (artifacts of embedding classical distributions into Hilbert space), others persist under physicality constraints but remain compatible with classical models in an overlap regime, and only a final class requires genuinely nonclassical features. Making these levels explicit clarifies what different witnesses do and do not certify.

We first situate the discussion within the broader literature and motivate the operational perspective. We then use Gaussian systems as a warm-up, where second-moment structure and PPT-type tests are especially transparent. Building on this, we introduce three regimes for general systems and conclude with their operational meaning and practical implications. This chapter is based on our work in Ref. [5].

3.1. Motivation and framework

In recent years, novel attempts have been put forward to scale down the fundamental difference between classical and quantum theory by showing that certain features regarded as genuinely quantum can already be found in classical models if one imposes epistemic constraints [43–47], fundamental indeterminacy due to finite information [1, 48], classical-anti-classical toy models [49], or using operational probabilistic theories [50]. In particular, Refs. [1, 49, 50] have proposed ways to construct analogues of entanglement in their respective proposed classical models. Parallel to these developments, the debate on "classical entanglement" in optics has highlighted the formal equivalence between quantum entanglement and the non–separable coupling of different degrees of freedom (e.g., polarization and spatial modes) within a single classical electromagnetic field [51, 52]. These correlations,

however, are simply mathematical analogies and are operationally distinct from entanglement, which becomes relevant, when two distant subsystems are involved [53–55].

Yet, while these approaches can be insightful to understand certain theoretical features, they typically rely on extending or modifying the underlying theoretical framework, remaining toy theories, and proofs of principles to point out that entanglement *can* be constructed in classical frameworks. In contrast, the analysis here proposed will be strictly carried out within *the bounds of classical and quantum mechanics*. We show that apparent entanglement–like correlations can already emerge when the *same physics is expressed in a different representation*. Particularly, we will look at classical states in Hilbert space and quantum states in phase space via the Wigner–Weyl formalism (see Chapter 2) [56]. This lets us distinguish features that are mere formal artifacts from those that mark robust physical differences between the theories. Before introducing formal nonseparability tests, however, recall that such criteria quantify the correlations through the second moments of position and momentum observables [57]. They serve as diagnostics indicating whether subsystems can be described by separable probability distributions or not. Only later will we see that these same criteria can *signal entanglement when the underlying system is classical*. In particular, second moment criteria, such as covariance–based nonseparability tests [34], can indicate correlations that appear entangled when expressed in a different formalism. These signatures alone, however, are not sufficient to establish genuine quantum entanglement. In our framework, both classical phase space distributions and quantum states are represented by operators via the WW map. Only operators that are positive semidefinite correspond to physical states, in the sense that they yield consistent probabilities for all observables. What ultimately matters, therefore, is whether the operator associated with the state remains positive in the chosen representation. We show that this positivity requirement defines only the first boundary. A second boundary, given in phase space representation by Wigner–function negativity, further separates classically reproducible nonseparability from genuinely quantum entanglement. Throughout this chapter, we refer to *representational entanglement* as the appearance of entanglement–like correlations that emerge purely from representing classical states in Hilbert space, while *hybrid entanglement* refers to valid quantum nonseparability that can still be reproduced by classical phase space distributions.

Peres already emphasized that expressing classical dynamics in Hilbert space does not make it quantum [55]. In his analysis of the Liouvillian formulation, even two uncoupled harmonic oscillators can be written in a Schrödinger–like equation, yet the resulting Liouvillian exhibits unphysical features such as an unbounded spectrum. In the present chapter we pursue a similar goal but go beyond Peres' observation. By embedding both classical and quantum mechanics within

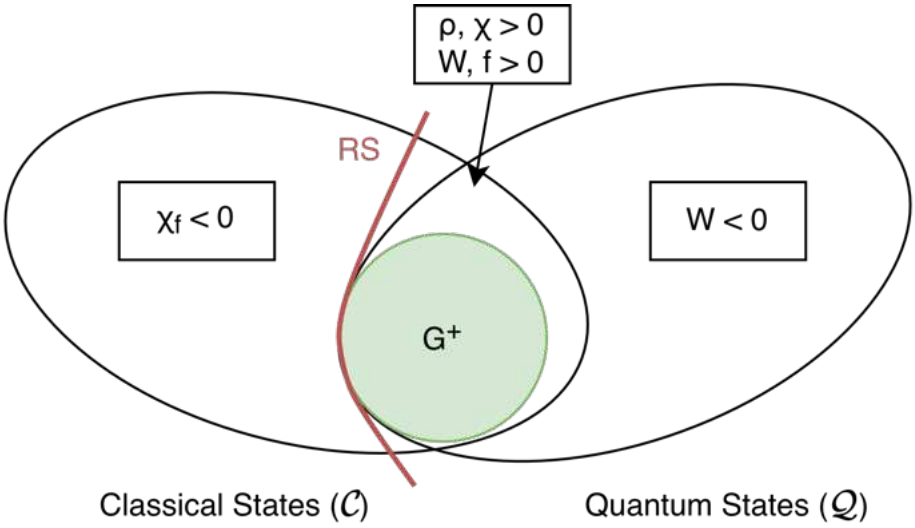

Figure 3.1.: Overlap of classical and quantum state spaces in the Wigner–Weyl representation. States in the intersection are operationally indistinguishable when access is restricted to phase space (quadrature) statistics.

the same single representational framework through the Wigner–Weyl transform introduced in Chapter 2, we make this distinction *operational*: only positive operators correspond to states that yield consistent statistics for all observables, while non–positive (classical) operators can reproduce correlations only under restricted, jointly measurable observables. Positivity, rather than a generic Hilbert space form, emerges as the genuine distinction between classical and quantum states. This criterion, however, although testable operationally (for example, via full state tomography), is not sufficient, since many classical states can satisfy it. Therefore, additional criteria are required. We show that operational signatures of measurement incompatibility (going beyond second moment quadrature data) and Wigner function negativity provide the operational criteria needed to identify the genuinely quantum regime. Figure 3.1 visualizes this boundary and the overlap where both coexist, setting the stage for the comparative analysis that follows.

3.1.1. Mapping and definitions

To express both classical and quantum mechanics within a common framework, we utilize the formalism given in Chapter 2. In particular, recall the definition of the Wigner transform of Eq. (2.35), which associates a quantum density operator $\hat{\rho}$ with its corresponding quasiprobability distribution $W_\rho(q,p)$ in phase space. Also note that the inverse transform, the Weyl map, in Eq. (2.13) transforms a phase space distribution $f(q,p)$ to its corresponding (pseudo-) density operator $\hat{\chi}_f$ in

Hilbert space. For further convenience, let us introduce the Stratonovich-Weyl kernel [58]

$$\hat{\Delta}(q,p) = \int_{-\infty}^{\infty} ds\, e^{\frac{i}{\hbar}ps}\, |q+\frac{s}{2}\rangle\, \langle q-\frac{s}{2}|\,, \tag{3.1}$$

with which the Weyl transform takes the more compact form

$$\hat{\chi}_f = W^{-1}[f] = \int_{-\infty}^{\infty} dq \int_{-\infty}^{\infty} dp\; f(q,p)\, \hat{\Delta}(q,p). \tag{3.2}$$

Since we are now primarily interested in the study of bipartite systems, we can immediately see that a classical phase space density $f(q_1,p_1,q_2,p_2)$ is mapped to

$$\hat{\chi}_f = \int dq_1\, dp_1\, dq_2\, dp_2\; f(q_1,p_1,q_2,p_2)\, \hat{\Delta}(q_1,p_1) \otimes \hat{\Delta}(q_2,p_2). \tag{3.3}$$

As we have discussed in Section 2.1.2, this construction leads to a one–to–one correspondence between normalized classical phase space densities f and trace–one operators $\hat{\chi}_f$ in Hilbert space, although these operators are not guaranteed to be positive, and thus do not in general represent valid quantum states. We denote these classical operators by $\mathcal{C}$ and the set of genuine quantum states by $\mathcal{Q}$. An operator $\hat{\chi}$ belongs to $\mathcal{C}$ if and only if its Wigner representation is everywhere non–negative. Equivalently, it arises from the Weyl transform of a classical probability density f. An operator $\hat{\rho}$ belongs to $\mathcal{Q}$ if and only if it is positive semidefinite.

Consequently, neither state space is contained in the other, i.e., $\mathcal{C}$ and $\mathcal{Q}$ are distinct, partially overlapping sets (as illustrated in Fig. 3.1). States in the intersection $\mathcal{C} \cap \mathcal{Q}$ (e.g., Gaussian states and, more generally, Wigner–positive mixed states) are operationally indistinguishable when the observer is restricted to phase space statistics accessible via quadrature (homodyne) measurements, equivalent to the expectation values of Weyl–ordered observables, obtained from measurements on identically prepared ensembles. In this regime, phase space data alone does not reveal whether a given state has a genuinely quantum origin or arises from a classical distribution. Moreover, some states in this intersection can exhibit entanglement in the typical Hilbert space sense. In other words, within this operator representation, one can push classical states so that they *satisfy both characteristic features of the quantum formalism:*

(A) *Positivity*: $\hat{\chi} \geq 0$ (and $\mathrm{Tr}\,\hat{\chi} = 1$),

(B) *Entanglement*: $\hat{\chi} \neq \sum_i p_i\, \hat{\chi}_A^{(i)} \otimes \hat{\chi}_B^{(i)}$, with $p_i \geq 0$, $\sum_i p_i = 1$, and each $\hat{\chi}_{A/B}^{(i)}$ satisfying (A).

While this possibility for classical states is clear from the standpoint of the formalism, one should place (A) and (B) on an operational footing suitable for laboratory testing. To this end, we imagine Alice and Bob, each performing phase–space measurements in their respective laboratories, who wish to test whether their shared system can exhibit entanglement (as in many quantum experiments, e.g., in nanomechanical systems [59, 60]). As our discussion shows, classical states can also exhibit this feature in the operator picture, provided they satisfy (A) and (B).

In practice, however, verifying (A) and (B) may require operationally demanding techniques (such as full state tomography in the worst-case scenario). What is typically done instead is to replace (A) and (B) by weaker, experimentally friendlier *necessary* conditions, such as covariance-based criteria:

(A*) *Uncertainty relations*, exemplified by the Robertson–Schrödinger relation [36, 37],

(B*) *Positive-partial-transpose (PPT) criterion*, which for continuous-variable bipartite systems reduces to the Duan–Simon criterion formulated in terms of second-order moments (see, e.g., [33, 34, 37, 57])

In the following section, we shall analyze these tests in detail for the Gaussian case and consequently show how they can fail for non-Gaussian systems, leading us directly to the definition of representational entanglement.

3.2. Gaussian systems: covariance criteria and their limitations

We begin with Gaussian states as a warm–up, not because they are the most general case, but because they make the operational content of correlation criteria unusually clear. In the Gaussian setting, restricting attention to second moments (i.e., (A*) and (B*)) is not merely a convenience, but it is the whole description. This allows us to clearly separate what can be inferred from covariance data alone from what would require additional information. The goal of this section is to show how nonseparability can appear at the level of representation under restricted access and why it demands a more careful classification that remains meaningful beyond Gaussianity.

3.2.1. Classical Gaussian nonseparability

Before applying separability tests, we must ensure that the Hilbert space representative associated with a classical Gaussian distribution satisfies the minimal

consistency requirements of the framework (in particular, the appropriate positivity/physicality condition (A*)). The next lemma isolates these conditions in a form that can be checked directly from the covariance matrix and will serve as the main technical tool for the example.

Lemma 1 (Valid density operator)
A Weyl-mapped operator $\hat{\chi}$ is a valid density operator (positive semidefinite and $Tr[\hat{\chi}] = 1$), iff the corresponding covariance matrix Σ satisfies the RS uncertainty $\Sigma + \frac{i\hbar}{2}\Omega \succeq 0$ plus higher-moment conditions when non-Gaussian. (In the Gaussian case, the RS condition is necessary and sufficient.)

Proof. **RS is necessary for all physical states**
Let $\hat{\chi}$ be a physical density operator ($\hat{\chi} \geq 0$, $\mathrm{Tr}[\hat{\chi}] = 1$). Define the centered quadratures of the state as $\tilde{R}_i = R_i - \langle R_i \rangle$. For any complex vector $z \in \mathbb{C}^{2n}$, define the operator $L_z = z^\dagger \tilde{R} = \sum_j z_j^* \tilde{R}_j$. The positivity of $\hat{\chi}$ now implies that

$$\langle L_z L_z^\dagger \rangle \geq 0. \tag{3.4}$$

Using the simple relation

$$\tilde{R}_j \tilde{R}_k = \frac{1}{2}[\tilde{R}_j, \tilde{R}_k] + \frac{1}{2}\{\tilde{R}_j, \tilde{R}_k\}, \tag{3.5}$$

as well as $1/2\langle\{\tilde{R}_j, \tilde{R}_k\}\rangle = \Sigma_{jk}$ and $[\tilde{R}_j, \tilde{R}_k] = i\hbar\Omega_{jk}$, we find that

$$z_j^* \left(\Sigma_{jk} + \frac{1}{2} i\hbar\Omega_{jk}\right) z_k \geq 0, \quad \forall z. \tag{3.6}$$

Thus the RS condition is necessary for any physical state, as we have only used commutation relations and positivity. □

Proof. **RS is necessary and sufficient for Gaussian states**
Assume now that $\hat{\chi}$ is a Gaussian state. It is our goal to show that $\Sigma + \frac{i\hbar}{2}\Omega \geq 0$ implies $\hat{\chi} \geq 0$. To prove this, we have to use Williamson's theorem (see Sec. 2.3.2), which allows us to symplectically diagonalize the covariance matrix of the system

$$\Sigma = S^T D S, \quad \text{with} \quad D = \mathrm{diag}(\nu_1, \ldots, \nu_n), \tag{3.7}$$

where $\nu_i > 0$ are the symplectic eigenvalues of the covariance matrix. Note, however, that the symplectic transformation S, corresponding to a unitary U_S, acting on the state, leaves the RS condition invariant, making it equivalent to

$$D + \frac{i\hbar}{2}\Omega \succeq 0. \tag{3.8}$$

Now a Gaussian state with diagonal covariance D can be considered a tensor product of thermal states $\tau = \tau_1 \otimes \cdots \otimes \tau_n$ [61]. So for each mode, the single mode covariance ν_j corresponds to a thermal state τ_j with a mean occupation number

$$\bar{n}_j = \frac{\nu_j}{\hbar} - \frac{1}{2} \geq 0 \Longleftrightarrow \nu_j \geq \frac{\hbar}{2}. \tag{3.9}$$

Thus, if $\nu_j \geq \frac{\hbar}{2}$, each mode is a valid positive density operator. Undoing the symplectic transformation from before via the unitary U_S, we obtain a positive Gaussian density operator

$$\hat{\chi} = U_S \tau U_S^\dagger \tag{3.10}$$

Combining the necessity from before with this sufficiency tells us that a Gaussian density matrix that satisfies the RS condition is a physical state ($\hat{\chi} \geq 0$). □

We have proven in the lemma that the Robertson–Schrödinger (RS) matrix inequality $\frac{i\hbar}{2}\Omega \succeq 0$ is a necessary condition for any positive density operator and that for Gaussian operators it is also sufficient. Note that we have only used positivity and the commutation relations. Now, this gives us an immediate diagnostic tool. Covariance data alone can confirm that a Weyl–mapped operator $\hat{\chi}_f$ *cannot* be a physical quantum state whenever the RS criterion fails. This means that it separates the Gaussian states that satisfy the uncertainty relations (G^+ in Fig. 3.1) from those that do not. This can now be used to separate two distinct possibilities when applying the PPT test to $\hat{\chi}_f$, (i) a genuine entanglement signal, which only occurs when $\hat{\chi}_f$ is a bona–fide density operator and Σ^Γ violates the PPT criterion (see Sect. 2.3.2); and (ii) a spurious PPT signal, which occurs when Σ^Γ would be read as "entangled" by the covariance–based test, while $\hat{\chi}_f$ itself is non–positive. The following theorem formalizes the existence of such spurious signals in the Gaussian case.

Theorem 2 (Existence of Gaussian nonseparability from classical phase space distributions)
Let $f(q,p) \geq 0$ be a normalized classical phase space probability density on $\mathbb{R}^4$, and let $\hat{\chi}_f := \int f(q,p)\hat{\Delta}(q,p)\,dq\,dp$ be the operator obtained by the Weyl transform. Denote by Σ the covariance matrix of $\hat{\chi}_f$ and by Σ^Γ the covariance after partial transposition on mode/system 2.

Then there exists a choice of f such that

1. $\Sigma^\Gamma + \frac{i\hbar}{2}\Omega \not\succeq 0$ *(PPT covariance test flags the state as entangled), while*
2. $\Sigma + \frac{i\hbar}{2}\Omega \not\succeq 0$ *(so $\hat{\chi}_f$ violates the RS inequality and therefore cannot be a positive density operator, i.e., lying within the $\mathcal{C}$-set).*

Consequently, the PPT test applied to $\hat{\chi}_f$ may indicate "entanglement" even though $\hat{\chi}_f$ is not a physical quantum state, making this indication non-operational.

Additionally, in the Gaussian case, the two matrix inequalities are equivalent to positivity statements. The second condition above is equivalent to $\hat{\chi}_f$ having at least one negative eigenvalue, so the theorem yields explicit parameter regions in which classical Gaussian correlations trigger a spurious PPT signal.

Note that this theorem relies on the necessity part (positivity → RS) of Lemma 1. We will now proceed to prove the theorem for the Gaussian family by analytic computation of the symplectic eigenvalues and then illustrate it numerically. After the Gaussian case, we extend the discussion to selected non-Gaussian classical distributions to show the same logical structure.

To give physical meaning to the system we use in the proof, consider two 1D particles (or oscillators), each described by position x_i and momentum p_i. Furthermore, their statistics are Gaussian, and each particle has the same variance in position and momentum $\mathrm{Var}(x_1) = \mathrm{Var}(x_2) = \mathrm{Var}(p_1) = \mathrm{Var}(p_2) = s$. Both positions and both momenta are correlated with the same covariance k, making the covariance matrix of the system

$$\Sigma = \begin{pmatrix} s & 0 & k & 0 \\ 0 & s & 0 & k \\ k & 0 & s & 0 \\ 0 & k & 0 & s \end{pmatrix}. \tag{3.11}$$

We can also consider this system to be two masses on springs, each subject to *thermal noise plus a common random external force*. The thermal noise makes each variance s, and the common force gives rise to cross-correlations k between the particles' displacements and between their velocities (momenta). Since the force couples equally to both, the correlation structure is symmetric.

Proof. **Existence of classical Gaussian nonseparability**
We consider the family of two-mode classical Gaussian distributions with zero mean and a covariance matrix like in eq. 3.11, where $s > 0$, $|k| < s$. This structure enforces identical variances for all quadratures and identical correlations between the two modes. By the Weyl map, symmetrized second moments are preserved, meaning that the same Σ matrix is the covariance of the Weyl-mapped operator $\hat{\chi}_f$.

To test positivity, we compute the symplectic spectrum of Σ, which can be done by computing the eigenvalues of the matrix $|i\Omega\Sigma|$, where the absolute value indicates that the positive eigenvalue is taken and Ω represents the symplectic form from Eq. (2.45). Short calculation yields

$$\nu_1 = s + k \quad \nu_2 = |s - k|. \tag{3.12}$$

Similarly, for the partially transposed covariance Σ^Γ one finds instead

$$\tilde{\nu} = \sqrt{s^2 - k^2}. \tag{3.13}$$

The Robertson-Schrödinger condition requires

$$\nu_1 \geq \frac{\hbar}{2}, \quad \nu_2 \geq \frac{\hbar}{2}, \tag{3.14}$$

while for the partially transposed covariance Σ^Γ one would require

$$\tilde{\nu} \geq \frac{\hbar}{2}. \tag{3.15}$$

There exist parameter choices, such that both inequalities cannot be satisfied simultaneously. Take, for instance, $s = 0.6$, $k = 0.4$ and $\hbar = 1$. Then

$$\nu_1 = 1, \quad \nu_2 = 0.2, \quad \tilde{\nu} = \sqrt{0.6^2 - 0.4^2} \approx 0.447, \tag{3.16}$$

that means that both ν_2 and $\tilde{\nu}$ are strictly below $\hbar/2$. Reminding ourselves of the fact that for Gaussian states, the RS condition is necessary and sufficient for positivity, the operator $\hat{\chi}_f$ corresponding to this classical distribution cannot be positive. At the same time, the partially transposed covariance Σ^Γ also fails the inequality and would therefore be declared as entangled by the PPT criterion.

We therefore conclude that the PPT indication is of a spurious nature for this classical probability distribution f, because the Weyl-transformed operator $\hat{\chi}_f$ is not a valid quantum state, and no entanglement claim is meaningful. □

We can further analyze this symmetric two–mode distribution by plotting the available parameter space for the (s, k) pairs. Of particular interest for this discussion is the red region in Figure 3.2, where the RS condition fails and the PPT condition gives an entanglement signal. Note, however, that this example is of purely pedagogical value, as the covariance data that would flag a PPT signal, also immediately indicates the unphysical nature of the obtained density operator. But by extending this treatment to non–Gaussian states, we can reveal a more subtle structure and define *representational entanglement*. In the next section, we will briefly discuss how and why this procedure has to be adapted in the non–Gaussian regime by considering a non–Gaussian example and showing the failure of the RS condition in this case.

3.2.2. Beyond the Gaussian case: RS without positivity

In the Gaussian setting, the RS inequality is both necessary and sufficient for positivity. Outside the Gaussian family of states, however, RS is only necessary.

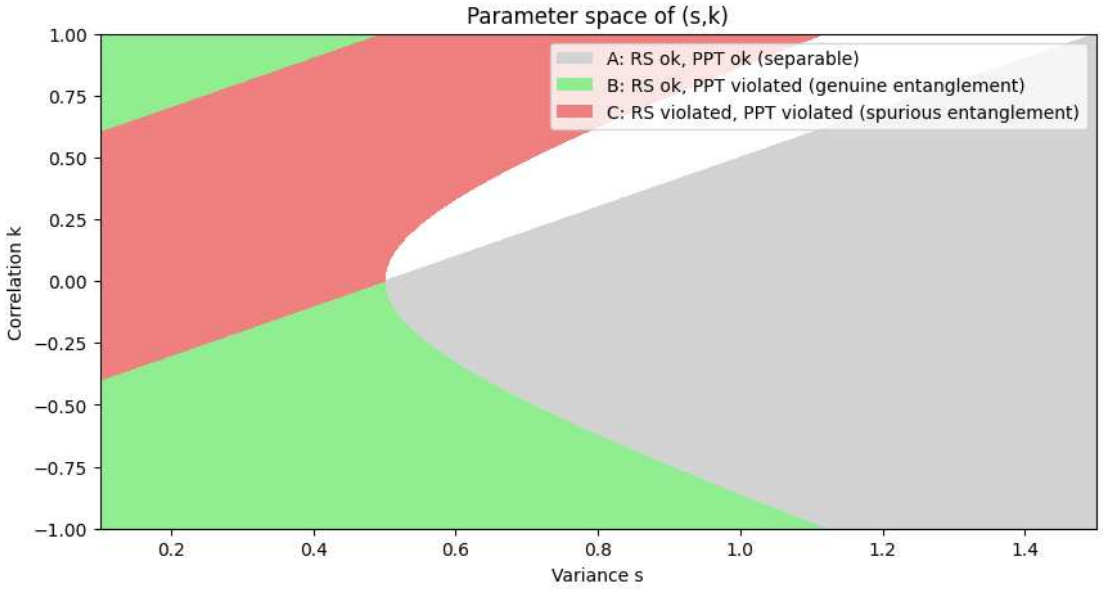

Figure 3.2.: Parameter space of two-mode symmetric Gaussian classical distribution in terms of the local variance s and the correlation k (units $\hbar = 1$). The shading shows three qualitatively distinct regimes as determined by the symplectic eigenvalues of the original covariance Σ and of the partially transposed covariance Σ^{Γ}. Gray (Region A): both RS and PPT inequalities are satisfied, so the Weyl-mapped operator is positive and separable. Green (Region B): The RS inequality holds while the PPT inequality is violated, indicating genuine entanglement of a physical Gaussian state. Red (Region C): both the RS inequality and the PPT inequality are violated. In this regime the Weyl-mapped operator is non-positive, while the PPT test would incorrectly signal entanglement.

Higher–order moments may still render the Weyl–mapped operator non–positive, even if the covariance appears consistent. To illustrate this limitation, we consider a simple non–Gaussian distribution: a mixture of two displaced Gaussians with equal weights.

We start from a separable diagonal covariance

$$\Sigma_0 = \mathrm{diag}[\sigma_{xA}^2, \sigma_{pA}^2, \sigma_{xB}^2, \sigma_{pB}^2] \tag{3.17}$$

describing the two modes A and B of some classical system. The non-Gaussianity is realized by displacing the sum of two separate Gaussians by

$$\mu_{\pm} = (\pm d, 0, 0, 0). \tag{3.18}$$

The classical phase space probability distribution of this mixture, can then be

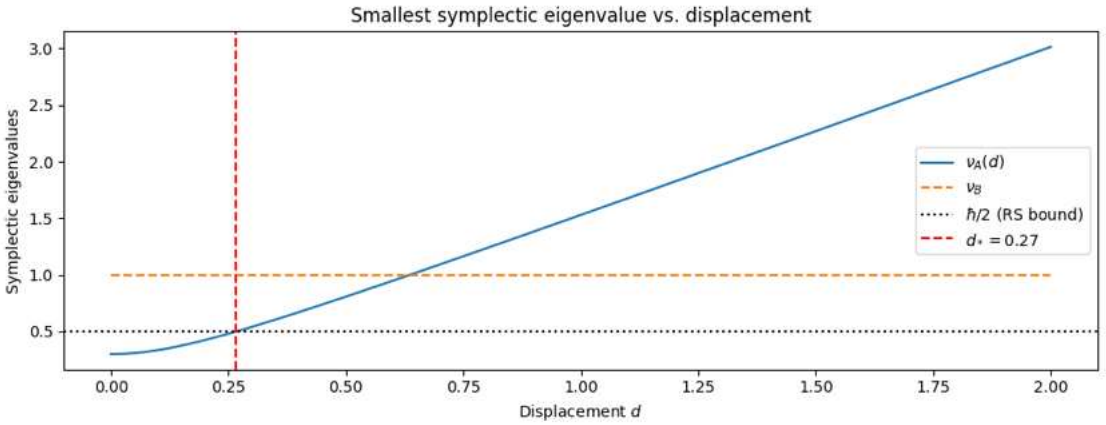

Figure 3.3.: Symplectic eigenvalue of the displaced two-mode mixture as a function of displacement d in mode A. The eigenvalue $\nu_A(d) = \sigma_{pA}\sqrt{\sigma_{xA}^2 + d^2}$ grows with d, while $\nu_B = \sigma_{xB}\sigma_{pB}$ remains constant. The RS condition requires $\nu_{\min}(d) \geq \hbar/2$. For small d, $\nu_A(d) < \hbar/2$ so the mapped operator fails RS. Beyond the threshold d_* (red dashed line), the mixture covariance satisfies RS even though each Gaussian component is nonphysical. This demonstrates explicitly how a non–Gaussian mixture can yield a covariance matrix that is consistent with RS, while the underlying operator is non–positive.

defined as

$$P(x) = \frac{1}{2}G(x;\mu_+,\Sigma_0) + \frac{1}{2}G(x;\mu_-,\Sigma_0), \tag{3.19}$$

where $G(\,.\,;\mu,\Sigma_0)$ denotes a Gaussian density with mean μ and covariance Σ_0. The covariance of this mixture can be decomposed in the covariance of the individual systems Σ_0 plus a "between component" of the form $1/4(\mu_+ - \mu_-)(\mu_+ - \mu_-)^T$. The total covariance then becomes

$$\Sigma = \mathrm{diag}[\sigma_{xA}^2 + d^2, \sigma_{pA}^2, \sigma_{xB}^2, \sigma_{pB}^2]. \tag{3.20}$$

And since the covariance is block diagonal in the modes A and B, the symplectic eigenvalues can simply be read off to be

$$\nu_A(d) = \sigma_{pA}\sqrt{\sigma_{xA}^2 + d^2}, \quad \nu_B = \sigma_{xB}\sigma_{pB}. \tag{3.21}$$

Here we can already observe that if $\nu_A(0) < \nu_B$, the minimal eigenvalue is $\nu_A(d)$, which increases with d, as seen in Fig. 3.3. This makes it such that the original covariance matrix could fail to satisfy the RS condition, but the displaced covariance can be made to satisfy the condition by choosing d appropriately. In this case,

there exists a threshold displacement

$$d_* = \sqrt{\left(\frac{\hbar}{2\sigma_{pA}}\right)^2 - \sigma_{xA}^2} \tag{3.22}$$

beyond which $\nu_A(d) \geq \hbar/2$ and the RS condition is satisfied. In the other case, where $\nu_B < \nu_A(0)$, the minimum eigenvalue is always ν_B and varying the displacement d has no effect on the RS condition.

So far our analysis has been based solely on the covariance matrix. To see whether the operator is actually negative, it is instructive to construct the full operator. Using the Weyl-kernel from Eq. 3.1, the position basis matrix element of each displaced Gaussian can be written in a closed form

$$\rho_G(x, y, d) = \frac{1}{(2\pi)^{3/2}\hbar\sigma_x} \exp\left[-\frac{\left(\frac{x+y}{2} - d\right)^2}{2\sigma_x^2}\right] \exp\left[-\frac{\sigma_p^2}{2\hbar^2}(x-y)^2\right]. \tag{3.23}$$

For our two–mode system, where only mode A is displaced, the kernels factorize (no inter–mode correlations) as

$$\rho_{AB}^{(\pm)}(x_A, x_B; y_A, y_B) = \rho_G^A(x_A, y_A; \pm d)\, \rho_G^B(x_B, y_B; 0). \tag{3.24}$$

The non–Gaussian mixture of Eq. 3.19 remains an equal mixture in Hilbert space of the form

$$\rho_{AB} = \frac{1}{2}\left(\rho_{AB}^{(+)} + \rho_{AB}^{(-)}\right). \tag{3.25}$$

We then diagonalize the resulting operator numerically on a finite grid (see Appendix A.1 for a detailed calculation of the matrix element and the numerical diagonalization). The smallest eigenvalue $\lambda_{\min}(d)$ is compared to the smallest symplectic eigenvalue $\nu_{\min}(d)$. As shown in Fig. 3.4, there exists a region of displacements where the RS inequality is satisfied ($\nu_{\min} \geq \hbar/2$), but the operator has negative eigenvalues ($\lambda_{\min} < 0$). This confirms directly that covariance data alone is no longer sufficient for the non-Gaussian case.

Importantly, the covariance of this mixture can be tuned such that the RS condition is satisfied for sufficiently large displacement d. At the covariance level, the system therefore appears "quantum–allowed." However, the Weyl-mapped operator constructed from the full distribution remains non-positive, since higher-order moment constraints are violated. This shows that, unlike in the Gaussian case, RS compliance is not sufficient to guarantee physicality in the non-Gaussian regime.

This example highlights a very fundamental limitation of restricting the diagnostics to only covariance data outside the Gaussian family. While in Gaussian

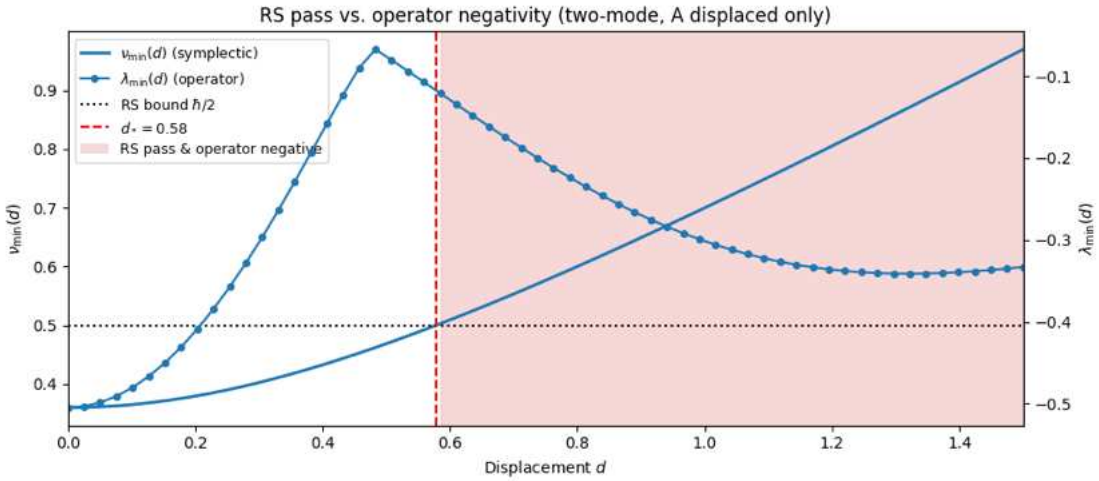

Figure 3.4.: Smallest symplectic eigenvalue $\nu_{\min}(d)$ (solid blue, left axis) and smallest density operator eigenvalue $\lambda_{\min}$(d) (markers, right axis) for the two–mode displaced mixture (displacement on mode A). Parameters: $\sigma_{xA} = 0.6$, $\sigma_{pA} = 0.6$, $\sigma_{xB} = 1.0$, $\sigma_{pB} = 1.0$, $\hbar = 1$. The dashed line indicates the RS bound $\hbar/2$. The vertical line marks the threshold displacement d_* of Eq. 3.22, where $\nu_A(d)$ first reaches the RS bound. The shaded region highlights values of d where the RS condition is satisfied, yet the operator is negative. This explicitly demonstrates that RS compliance is not sufficient for positivity outside Gaussian systems.

systems the RS inequality coincides with physicality, non-Gaussian systems can evade this equivalence. For example, RS may hold, and PPT might suggest entanglement, yet the underlying operator is not positive, giving *representational entanglement*. Such cases demonstrate that covariance–based entanglement criteria cannot be naively extended beyond the Gaussian regime. In particular, any claim of entanglement in non-Gaussian systems must be supplemented by explicit checks of operator positivity. We will now proceed by formalizing another form of classical nonseparability, where the covariance criteria (A*) and (B*) will suggest genuine entanglement, while the underlying operator is non-positive.

3.3. Representational entanglement (RE): nonseparability without positivity

Now that we have studied the usefulness and limitations of covariance-based criteria (A*) and (B*) of Section 3.1, we can turn towards a more interesting form of nonseparability. Assume that the observer of our bipartite system only has limited access. Such limitations can be fundamentally built into the model, either via epistemic restrictions in the spirit of Spekkens [43], or in frameworks with fundamental indeterminacy [48], where access to complete information about the system is not possible. In contrast, we shall now focus solely on experimental constraints, such as access only to the second moments of position and momentum, which are nevertheless sufficient to test conditions (A*) and (B*). We will show that for this restricted setup, non-Gaussian classical states can satisfy RS and even violate PPT at the covariance level, while their associated operator fails positivity and thus does not correspond to a physical quantum state. This subtle behaviour will now be formally defined:

Definition 3.1. Representational entanglement (RE):
A bipartite Weyl-mapped operator $\hat{\chi}$ (trace one) with its corresponding covariance matrix Σ exhibits representational entanglement if:

- $\hat{\chi} \in \mathcal{C}$,
- $\hat{\chi} \not\succeq 0$ (non-positive),
- $\Sigma + \frac{i\hbar}{2}\Omega \succeq 0$ (satisfying RS),
- but $\Sigma^{\Gamma} + \frac{i\hbar}{2}\Omega \not\succeq 0$ (violating covariance–based PPT).

So if $\hat{\chi}$ were assumed to be a density operator, it would be flagged as entangled by covariance based criteria. These states occupy the RE region in Fig. 3.6.

To find an example of *representational entanglement*, consider the mixture of two Gaussians G yielding a non-Gaussian state where the displacements cancel on average but contribute additional variance to the covariance matrix

$$P(z) = \frac{1}{2}\left[G(z, \mu_+, \Sigma_0) + G(z, \mu_-, \Sigma_0)\right]. \tag{3.26}$$

To construct the covariance matrix Σ of the mixture, we recall that the covariance of a mixed state consists of two contributions: the *internal variance* within each component and the *variance of the component means*. For our mixture centered around $\mu_\pm = (\pm d, \mp d, 0, 0)$, both Gaussians share the same internal covariance Σ_0, while their means are displaced symmetrically around the origin. The overall covariance is therefore

$$\Sigma = \Sigma_0 + \mathrm{Cov}[\mu_\pm] = \Sigma_0 + \frac{1}{4}(\mu_+ - \mu_-)(\mu_+ - \mu_-)^T. \tag{3.27}$$

Intuitively, the second term represents the additional spread originating from mixing two displaced components. Writing this out explicitly, for $z = (q_A, q_B, p_A, p_B)$, with intra-mode variances s_q, s_p and inter-mode correlations k_q, k_p we obtain

$$\Sigma = \begin{pmatrix} s_q + d^2 & k_q - d^2 & 0 & 0 \\ k_q - d^2 & s_q + d^2 & 0 & 0 \\ 0 & 0 & s_p & k_p \\ 0 & 0 & k_p & s_p \end{pmatrix}. \tag{3.28}$$

Note that for $d = 0$ the mixture reduces to a single Gaussian state, where RS and PPT are both necessary and sufficient. Furthermore, any two–mode covariance matrix can be brought into this form via local single–mode symplectic transformations [37]. The state is entangled if and only if it violates PPT while satisfying RS. At $d > 0$ the state becomes non–Gaussian, and although the covariance matrix may still satisfy RS and violate PPT, the underlying operator is non–positive and the emerging entanglement is purely *representational*.

As it is our goal to construct an example that is *not* "quantum–allowed", we need to make sure that the original Σ_0 fails the RS condition (although this condition is no longer necessary *and* sufficient, it is a good indicator for negativity in this setup). This means that the smallest symplectic eigenvalue $\nu^0_{\min}$ of Σ_0 has to satisfy

$$\nu^0_{\min} = \sqrt{k_p k_q + s_p s_q - |k_p s_q + k_q s_p|} < \frac{\hbar}{2}. \tag{3.29}$$

Note that there are always two different symplectic eigenvalues, but in this case they yield the same condition (see Appendix A.2). For the second criterion of Def. 3.1, we need to tune the displacement d in a way, that recovers RS compliance

for Σ. One can observe that only one of the two symplectic eigenvalues $\nu_1, \nu_2(d)$ of the total covariance is d–dependent. Therefore, we need to make sure that the smallest eigenvalue is $\nu_2(d)$ (enforcing $\nu_2(0) < \nu_1$) and ensure that ν_1 is not violating RS (enforcing $\nu_1 > \hbar/2$). Locking these conditions down and assuming that $s_p - k_p > 0$, allows us to find a threshold displacement like in Eq. 3.22

$$d_* = \frac{1}{2}\left[\frac{(\hbar/2)^2}{s_p - k_p} - (s_q - k_q)\right]. \tag{3.30}$$

Note that by setting the correlations k_q, k_p to zero, we fully recover Eq. 3.22 up to a factor of 1/2, which originates from the displacement of *both* modes. Finally, for the partially transposed covariance Σ^Γ it is a priori not clear, which of the symplectic eigenvalues is smallest and has to be checked once numerical values are inserted. A more detailed calculation and the explicit eigenvalues can be found in Appendix A.2.

To check the negativity of the resulting operator, we are required to compute the position–space representation of the Gaussian state in Hilbert space. For a two–mode Gaussian state with a shared covariance $\Sigma_0 = \left(\begin{smallmatrix} Q_0 & 0 \\ 0 & P_0 \end{smallmatrix}\right)$ and displacement $\mu_\pm = (\bar{q}_\pm, 0)$, the density operator in position basis can be written as a Gaussian kernel. Performing the Gaussian integral over the momenta (as shown in Appendix A.3), one obtains

$$\begin{aligned} K(x, y; \mu_\pm, \Sigma_0) &= \langle x_A, x_B | \, \rho_\pm \, | y_A, y_B \rangle \\ &= \frac{1}{(2\pi)\sqrt{\det Q_0}} \exp\left[-\frac{1}{2}(m - \bar{q}_\pm)^T Q_0^{-1} (m - \bar{q}_\pm)\right] \exp\left[-\frac{1}{2\hbar^2}\Delta^T P_0 \Delta\right], \end{aligned} \tag{3.31}$$

where $m = \frac{1}{2}(x + y)$, $\Delta = x - y$, and $\bar{q}_\pm = (\pm d, \mp d)$. For the classical mixture of the two displaced Gaussians, the total kernel is then simply

$$\langle x | \, \rho \, | y \rangle = \frac{1}{2} K(x, y; \mu_+, \Sigma_0) + \frac{1}{2} K(x, y; \mu_-, \Sigma_0). \tag{3.32}$$

We can discretize this kernel on a lattice, as it was done in Appendix A.1 and check it for negativity. Doing this and combining it with the criteria of the symplectic eigenvalues above allows us to make comparative statements.

In Fig. 3.5, we compare the two diagnostics of physicality. The upper panel 3.5a shows the smallest symplectic eigenvalues of the covariance matrices $\Sigma(d)$ and $\Sigma^\Gamma(d)$ as functions of the displacement d. For small displacements, $\Sigma(d)$ violates the RS condition, but as d increases, the eigenvalue surpasses the bound of 1/2, indicating that the displaced covariance is consistent with a valid Gaussian state. After partial transposition, however, the smallest eigenvalue remains below said bound, signaling entanglement via the PPT test. The shaded region highlights the

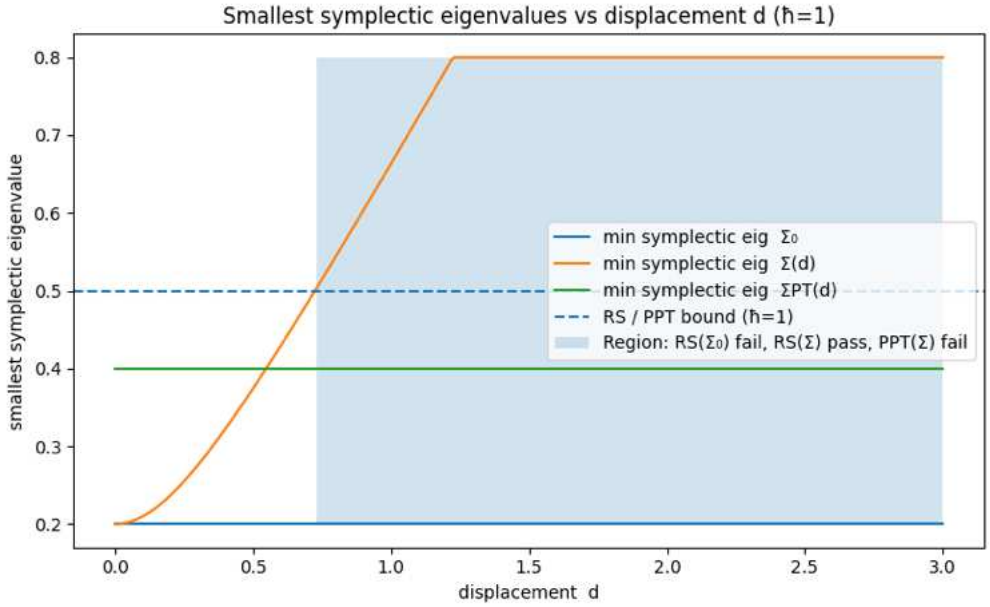

(a) Smallest symplectic eigenvalues of the covariance matrices Σ_0 (without displacement), $\Sigma(d)$ (with displacement included in the covariance), and $\Sigma^{\Gamma}(\mathrm{d})$ (after partial transposition), plotted against the displacement parameter d. The dashed horizontal line marks the Robertson-Schrödinger bound $\nu = 1/2$ (for $\hbar = 1$). When the smallest eigenvalue of Σ_0 drops below the bound, the original Gaussian would be unphysical. Including the displacement restores covariance–based physicality, indicated by $\nu(\Sigma) \geq 1/2$. After partial transposition, the smallest eigenvalue can again fall below $1/2$, signaling entanglement via the PPT criterion. The shaded region highlights values of d where $RS(\Sigma_0)$ is violated, $RS(\Sigma)$ is satisfied, and $PPT(\Sigma)$ is violated.

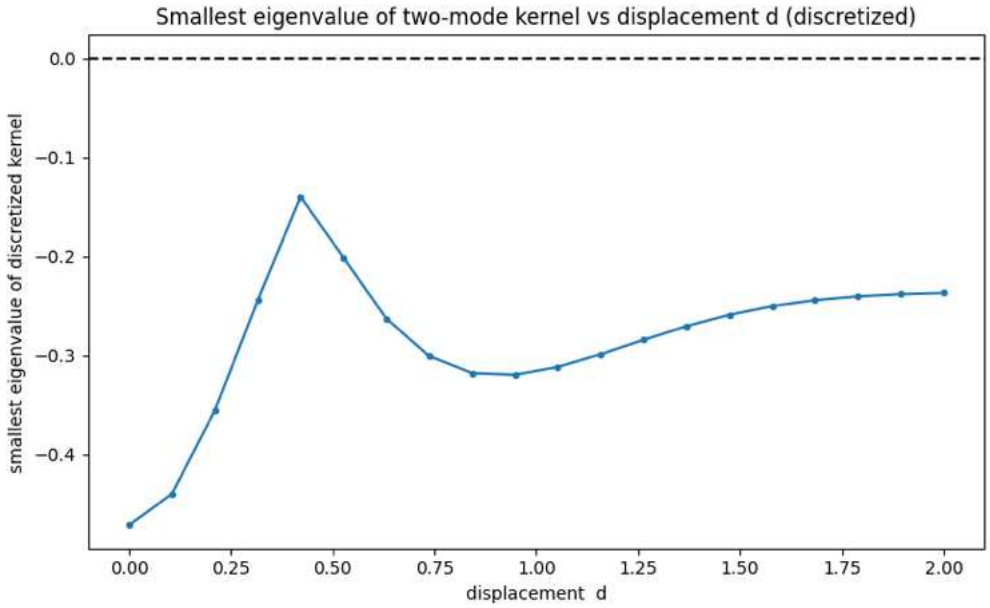

(b) Smallest eigenvalue of the discretized two-mode kernel operator, obtained from the explicit position-space representation of the displaced Gaussian mixture (Eq. 3.32) with respect to the displacement d. Negative values indicate that the operator is not positive semi-definite, i.e., that the constructed state is non-physical.

Figure 3.5.: Comparison of symplectic eigenvalues and kernel spectrum as a function of displacement d for $s_q = s_p = 0.5$ and $k_q = k_p = 0.3$.

values of d where $\Sigma(d)$ passes RS, while still violating PPT, giving *representational entanglement*.

The lower panel 3.5b on the other hand, shows the smallest eigenvalue of the density operator kernel, obtained by discretizing the position–space matrix elements of the displaced mixture. This eigenvalue is negative for all d indicating that the kernel does not lead to a positive semidefinite operator. Although the covariance matrix $\Sigma(d)$ appears to be valid, and even entangled, the actual state constructed from the displaced mixture is not physical.

Together, the plots in Fig. 3.5 illustrate the point we want to make here. Covariance–based criteria are not sufficient to guarantee that the underlying operator is non–negative. The kernel spectrum reveals negativity that is invisible at the covariance level. This negativity persists across all possible displacement values, even though the covariance–based criteria would suggest a physically acceptable entangled state for sufficiently large d. This is precisely what we call *representational entanglement*: a regime in which classical correlations, once recast in Hilbert space and viewed under restricted access, mimic the signatures of genuine quantum entanglement, without constituting a genuine quantum resource [1, 62]. This effect arises because the observer is still limited to second–moment information. Within this restricted view, entirely classical mixtures can reproduce the same covariance signatures that, in the quantum formalism, would be interpreted as entanglement.

3.4. Hybrid entanglement (HE): entanglement in the classical–quantum overlap

We now lift the observational restrictions of the previous section and allow the observer to test the operator positivity condition (A), i.e., to determine whether the state corresponds to a positive semidefinite operator in Hilbert space. Operationally, we still assume that each experiment accesses only a single local phase space (quadrature) setting per mode, as in standard continuous–variable experiments. However, by repeating the experiment for many settings, one can reconstruct the underlying operator via homodyne tomography [63]. Concretely, one measures the rotated quadrature

$$x_\phi = \cos\phi\, q + \sin\phi\ \ p, \qquad \phi \in [0, \pi), \tag{3.33}$$

which can be implemented by a phase space rotation $R(\phi)$ (e.g., harmonic evolution for an appropriate time) followed by a position measurement. Repeating this procedure yields the quadrature probability density $\mu_\phi(x)$, from which the Wigner function can be reconstructed

$$W_\chi(q,p) = \frac{1}{2\pi}\int_0^\pi d\phi \int_{-\infty}^{\infty} d\omega\ |\omega|\ e^{i\omega(q\cos\phi + p\sin\phi)}\,\tilde{\mu}_\phi(\omega), \tag{3.34}$$

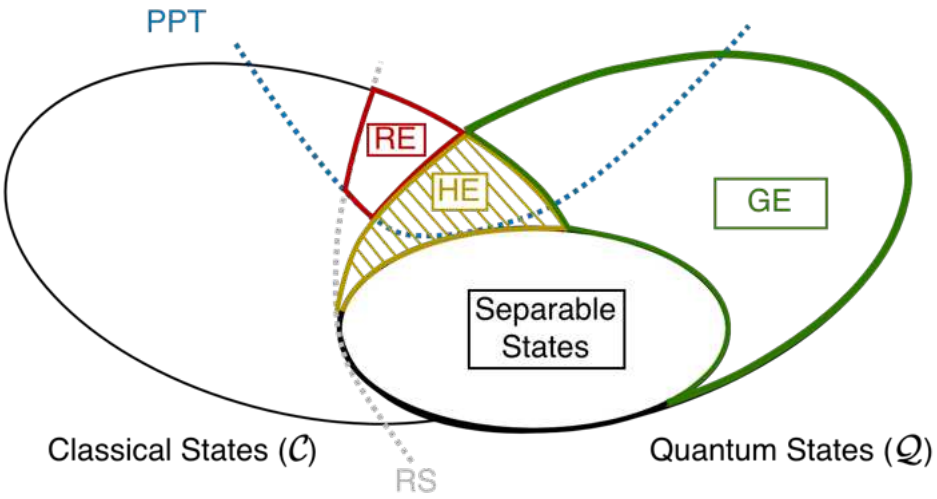

Figure 3.6.: Three regimes of nonseparability: (i) RE: representational entanglement (non-positive), (ii) HE: hybrid entanglement (classically reproducible), and (iii) GE: genuine entanglement (quantum-only).

where $\tilde{\mu}_\phi(\omega) = \int_{-\infty}^{\infty} dx\, e^{-i\omega x} \mu_\phi(x)$ is the Fourier transform of the measured marginal. Finally, the associated Hilbert space operator follows from the Weyl inversion in our convention,

$$\hat{\chi} = \frac{1}{2\pi\hbar} \iint dq\, dp\, W_\chi(q,p)\, \hat{\Delta}(q,p). \tag{3.35}$$

This reconstructed $\hat{\chi}$ can then be tested for positivity (e.g., via explicit diagonalization), eliminating the representational artifacts discussed above. In this way, one can arrive at the subset of states that satisfy (A) and are nonseparable according to the entanglement condition (B), while still being compatible with classical phase space models in the sense that they admit a positive phase space distribution. In other words, within the overlap $C \cap Q$, the same nonnegative Wigner function can be interpreted either as a classical probability distribution, or as the Wigner function of a positive density operator, and for phase space measurements, these two descriptions are operationally indistinguishable. We refer to nonseparability within this intersection as *hybrid entanglement*, corresponding to the HE region in Fig. 3.6. We shall further analyze the structure of such a set and properly define it as follows

Definition 3.2. Hybrid entanglement (HE):
A bipartite state ρ exhibits hybrid entanglement if

- $\rho \in \mathcal{Q}$ (positive, trace one),

- ρ is entangled in the usual Hilbert space sense, and
- $\rho \in \mathcal{C}$ (admits an everywhere nonnegative Wigner function), i.e. $\rho \in \mathcal{C} \cap \mathcal{Q}$.

Operationally, such states are entangled yet remain compatible with a classical phase space model under quadrature–access measurements.

Firstly, Gaussian entangled states populate this intersection, because their separability is fully characterized at the covariance level, and they remain operationally classical (in the sense discussed above) under measurements restricted to phase space (quadrature) observables [64]. To further explore this hybrid region, we shall go beyond Gaussian states. For pure states, we know that Gaussian quantum states saturate the entire classical–quantum overlap $\mathcal{C} \cap \mathcal{Q}$, as their corresponding Wigner function is positive [65]. For mixed states, however, this is no longer the case [66]. A simple example is the convex mixture

$$\rho(p) = p\,|0\rangle\langle 0| + (1-p)\,|1\rangle\langle 1|\,, \tag{3.36}$$

where the vacuum state corresponds to a positive Wigner function and the first excited Fock state exhibits Wigner function negativity. As p decreases, the contribution of the non–classical component increases, eventually driving the Wigner function negative for $p < 1/2$, as seen in Fig. 3.7. Thus the boundary between the hybrid and purely quantum region is at $p = 1/2$: for $p \in [1/2, 1]$ the state is non–Gaussian but Wigner–positive (hence classically compatible), while for $p < 1/2$ it necessarily lies within the genuinely quantum region.

This single–mode example shows that, for mixed states, the classical–quantum overlap $\mathcal{C} \cap \mathcal{Q}$ extends strictly beyond the Gaussian subset G_+: for $p \in [1/2, 1]$ the state $\rho(p)$ is non–Gaussian but still admits a nonnegative Wigner function everywhere. To obtain an entangled state in this overlap, we now embed $\rho(p)$ into a simple two–mode setting. This can be done by considering the following two-mode state $\rho_{\text{in}} = \rho(p) \otimes |0\rangle\langle 0|$, subjected to a balanced beamsplitter transformation and arriving at the following state

$$\begin{aligned} &\rho_{AB}(p) = p\,|0,0\rangle\langle 0,0| + (1-p)\,|\psi_+\rangle\langle\psi_+|\,, \\ &\text{with} \quad |\psi_+\rangle = \frac{|1,0\rangle + |0,1\rangle}{\sqrt{2}}. \end{aligned} \tag{3.37}$$

At the phase space level, a passive linear optical transformation like a beamsplitter is just a symplectic rotation of the quadratures; thus, it cannot create or remove Wigner function negativity. Hence, the two–mode Wigner function of $\rho_{AB}(p)$ is everywhere non-negative for the same parameter range $p \in [1/2, 1]$, in which the original single mode mixture $\rho(p)$ is Wigner–positive. In this range, $\rho_{AB}(p)$ is entangled for all $0 \leq p < 1$, and becomes separable only in the trivial limit $p \to 1$.

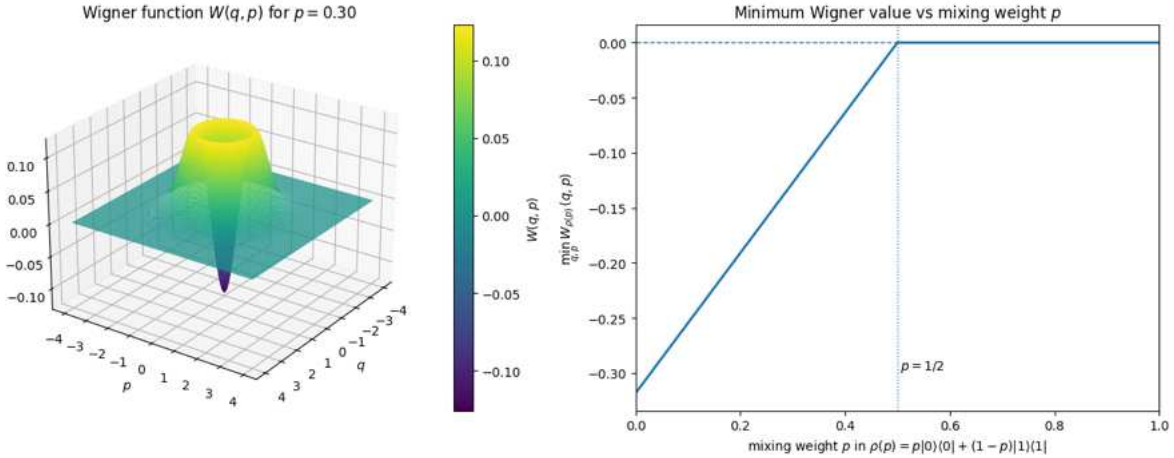

Figure 3.7.: Wigner negativity in a vacuum–single–photon mixture. Left: 3D surface of the Wigner function $W(q,p)$ for the mixed state $\rho(p) = p\,|0\rangle\langle 0| + (1-p)\,|1\rangle\langle 1|$ at a representative value $p = 0.30$, shown in dimensionless phase space coordinates (q,p). Right: minimum value of the Wigner function, $\min_{q,p} W_{\rho(p)}(q,p)$ as a function of the mixing weight p. The minimum becomes nonnegative at $p = 1/2$, indicating the disappearance of Wigner negativity, for a sufficiently large vacuum component.

Combining these facts, we obtain an illustrative example of *hybrid entanglement*: for

$$p \in [1/2, 1) \tag{3.38}$$

the state $\rho_{AB}(p)$ is non–Gaussian and entangled, yet still admits a positive Wigner representation and hence admits a classical phase space model. In the geometry of Fig. 3.6, it occupies the *HE* region inside the overlap $\mathcal{C} \cap \mathcal{Q}$.

Another example is our displaced two–mode Gaussian mixture of Eq. 3.26, which also provides an example of a state in the hybrid regime. For suitable choices of intra mode variances and inter mode correlations (for instance, $s_q = s_p = 1$, $k_q = 0.3$, $k_p = -0.8$), the resulting mixture is non–Gaussian, satisfies RS and violates PPT at the covariance level, and its Weyl–transformed operator is numerically found to be non–negative up to numerical precision. Detailed calculations for the beamsplitter example can be found in Appendix A.4.

So again, our hypothetical observer could not tell whether the source of these correlations is of classical or quantum mechanical nature, even if purely classical (RE) correlations are excluded. To collapse this hybrid intersection between classical and quantum correlations, we have to take one more step and allow our observer to test some form of non–classicality or allow for an explicit check of Wigner function negativity. This would finally remove all ambiguity and place the correlations in the quantum set, yielding *genuine entanglement.*

3.5. Genuine entanglement (GE): positivity plus nonclassicality

It is now our goal to move beyond the HE regime, where we have allowed full state tomography and found that positivity holds, but it is impossible for us to rule out any classical models via phase–space access alone, because the Wigner function remains positive. To obtain *genuine entanglement* (GE), we have to further remove the restrictions on the observer and allow an explicit test of measurement incompatibility or other non–trivial operations. One could, for instance, check the system's behavior under non–trivial dynamics like Kerr–type evolution [67], which would have no classical counterpart. Finally, it is the observer's goal to explicitly observe Wigner–function negativity, as this is a purely quantum feature and has no classical analogue. We have introduced this already in Section 2.3.3, where one could, for instance, use the negativity volume $\delta(W)$ as a witness for a non–classical signature. This allows a quantification of "how far outside of $\mathcal{C}$ we actually are". Formally, genuine entanglement can then be defined as follows:

Definition 3.3. Genuine entanglement (GE):
A state ρ exhibits genuine entanglement if

- $\rho \in \mathcal{Q}$ (it is a physical quantum state),
- ρ is entangled, and
- $\rho \notin \mathcal{C}$ (it lies outside the classical set, i.e., W_ρ takes negative values somewhere.)

This definition removes the ambiguity of the hybrid regime and places the correlations in the (GE) set of Fig. 3.6.

A good example for this would be the Fock state mixture of Eq. (3.37), where we have observed that the state is entangled for all $p < 1$ and hybrid entangled for $p \in [1/2, 1)$, and now genuinely entangled for $p < 1/2$, as shown in Fig. 3.7.

So generally, to certify genuine entanglement there are two routes one could take. To do static certification, for instance, requires tomography and a reconstruction of W, which would then allow for a computation of the negativity volume $\delta(W)$. A second, dynamical, certification can be done even when starting from Wigner–positive states. Certain nonlinear/non–Gaussian dynamics can generate negativity in the Wigner function. This will be especially important when we discuss gravity–mediated entanglement (GME) in more detail in the next chapter.

3.6. Discussion

This chapter introduced an operational hierarchy for "entanglement–like" correlations in Hilbert space representations of classical phase space states. The Gaussian analysis served as a controlled warm–up in which covariance–based criteria are transparent, while also illustrating how restricted access may produce misleading entanglement signals. Beyond Gaussianity, the hierarchy can be organized around two boundaries: first, positivity separates physical quantum states from representational artifacts, and second, nonclassicality (captured here by Wigner function negativity, or equivalently by leaving the classical set $\mathcal{C}$) separates states in the classical–quantum overlap from states that admit no classical phase space description. Our analysis shows that entanglement is not a unique feature of quantum theory, but can arise as a representational artifact or be mimicked by classical correlations in certain regimes.

These facts give rise to an interesting discussion: if an experiment and the corresponding phase space data analysis place the reconstructed state in the *HE* region, is the underlying system quantum or classical? From quadrature statistics alone, the answer is, in general, ambiguous, and additional criteria are required. One natural way to break this degeneracy is to probe the system under dynamics that go beyond quadratic Hamiltonians (i.e., genuinely non–Gaussian unitaries). Another interesting point was provided in Ref. [1], where it was emphasized that, although many quantum features—including entanglement—can already emerge in classical frameworks, it is ultimately the (in)compatibility between physical observables that fundamentally distinguishes classical from quantum physics. For example, to violate a Bell inequality, nonseparability alone is insufficient; one must measure incompatible observables. Here, we have shown that such incompatibility—specifically between position and momentum measurements—can be statistically emulated at the classical level simply by restricting an observer to a single phase space observable per experimental run. Remarkably, this reverses the narrative: incompatibility should be viewed as a necessary but not sufficient condition for detecting genuine quantumness. Our examples show that incompatibility is a reliable signature of quantumness only when paired with a particular class of genuinely quantum states (exhibiting Wigner-function negativity) or with genuinely non–Gaussian dynamics that drive hybrid entangled states out of the classical–quantum overlap into the GE regime.

Beyond their foundational relevance, our findings may play a crucial role in practical tasks such as detecting entanglement and reconstructing states in continuous–variable experiments. Covariance–based criteria such as Duan–Simon and Robertson–Schrödinger inequalities are widely used to certify entanglement from second moments of the quadratures [33, 34]. However, these criteria are strictly sufficient only within the Gaussian regime. When applied to non–Gaussian

continuous variable states, they may either fail to detect genuine entanglement or, conversely, signal spurious correlations, as we have shown here. The failure to detect genuine entanglement has been demonstrated in several works [68, 69]. Our results highlight a different limitation, as covariance–based witnesses may incorrectly certify nonseparability even when the underlying operator does not correspond to a physical quantum state. In this sense, ensuring operator positivity provides a simple and general diagnostic to distinguish physical entanglement from representational artifacts. Additionally, nonclassicality evidence, i.e., Wigner negativity or operational tests of measurement incompatibility, is required to move from the hybrid overlap $\mathcal{C} \cap \mathcal{Q}$ to the purely quantum domain.

4. Time Evolution and Gravity-Mediated Entanglement: Classical vs. Quantum Dynamics

In this chapter it is our goal to analyze the differences between classical and quantum time evolution in Hilbert space, when applied to an initial state that is typically used in gravity–mediated entanglement (GME) setups. We discuss to which order the gravitational potential has to be expanded to obtain quantifiable differences, compare the final states, and discuss the occurring negativity in the classical density matrix. This negativity in the classical von Neumann (CvN) evolution of Section 2.1.2 seems to suggest a deep link to the previous chapters and proposes a dynamical emergence of representational entanglement.

4.1. Gravity–mediated entanglement: state of the art and literature

Over roughly the last decade, a promising experimental setup has emerged, probing the interface of quantum information and gravity. *If two mesoscopic masses become entangled while solely interacting via gravity, then gravity must possess non–classical features.* In its simplest form, these proposals consider two masses prepared in spatial superpositions whose branches experience different Newtonian interaction phases, and if the masses are later measured and found to be entangled, the interaction that correlated them in the first place cannot be simulated by purely classical communication under "standard" locality assumptions. This gravity–mediated entanglement (GME) program was first independently proposed in 2017: one framed as an entanglement witness experiment with Stern–Gerlach interferometry [70], and the other framed as a general information–theoretic argument about the mediators [71].

These proposals are very promising in two ways. First, it suggests a table–top route to probing a genuinely gravitational degree of freedom without requiring

Planck–scale energies. Second, in entanglement generation, it seems to leverage a uniquely quantum informational feature, sidestepping ambiguities that often plague semi–classical descriptions. However, because entanglement is a statement about correlations between quantum systems, the strength of the inference "*entanglement implies quantumness of gravity*" depends strongly on which operations, assumptions, and models are admitted as "classical". A large body of literature therefore focuses not only on whether entanglement can be generated in idealized Newtonian models, but also on whether an alternative classical description could reproduce the same observational signatures.

From the modeling perspective, much of the early discussion treated gravity as an instantaneous Newtonian potential acting between two delocalized masses. Within this approximation, one can compute entanglement phases and identify parameter regimes in which the emerging entanglement is in principle observable. This picture has now been refined in several contexts. On the one hand, there are first–principle derivations from linearized quantum gravity that emphasize spacetime locality and a relativistic structure. A notable example is the path integral treatment [72], which makes explicit how entanglement is mediated by quantum features of the field and highlights the possibility of *retarded entanglement*, where correlations occur with a causal time delay, which would be impossible with an instantaneous interaction. On the other hand, there are systematic nonrelativistic expansions tailored to an experimentally realistic regime in which displacements are small compared to the separation. Kumar et al. develop a controlled "central-force" expansion and provide a general continuous–variable framework for quantifying entanglement generated by such interactions [73].

Parallel to these advances in the modeling, substantial efforts have gone into identifying and controlling non–gravitational noise and decoherence channels that could either suppress entanglement or generate false positives. Rijavec et al. provide a detailed analysis of how environmental decoherence impacts the viability of entanglement–based gravity tests, translating the abstract proposal to concrete experimental requirements on coherence times and isolation [74]. Related experimental design work explores how shielding and trapping can mitigate electromagnetic interactions, while keeping gravitational phases appreciable [75]. Beyond the original Stern–Gerlach interferometer, alternative platforms have been analyzed, including optomechanical and oscillator–based protocols [76–78].

A central source of debate running through this literature is concerned with the role of classicality assumptions. One influential line of work models a classical gravitational interaction as a classical information channel between the masses. In these "classical channel gravity" pictures, the interaction can reproduce certain mean-field effects, but necessarily introduces decoherence that prevents entanglement generation [79]. Closely related are semiclassical gravity models implemented via

measurement–and–feedback constructions, which can be consistent in the Newtonian regime while again implying decoherence constraints [80–82]. These approaches concretize the previous question: *if an experiment observes entanglement, which "classical" model classes does it actually exclude, and which loopholes remain?*

Motivated by this, recent work has explored signatures that go beyond "Gaussian entanglement" from quadratic Hamiltonians. Non–Gaussianity of matter can be used as a resource–theoretic witness, where, under certain assumptions, classical gravity cannot generate non-Gaussianity in the relevant quantum matter field dynamics, whereas a quantum gravitational interaction can [83]. This motivates experimental strategies that look specifically for the generation of non–Gaussian features, rather than relying solely on bipartite entanglement witnessing, which might turn out to be the way to go in the future. In parallel, there is a growing interest in tests of gravitational quantumness that do not rely on entanglement at all, for instance, via bounds on LOCC–simulation fidelity [84].

Finally, the field is currently experiencing an active debate on the "entanglement implies quantumness" statements and the corresponding no–go theorems. A claim by Aziz and Howl argues that, when matter is treated at the level of quantum field theory, local classical theories of gravity may still transmit some form of quantum information and thus generate entanglement through mechanisms not captured by the standard nonrelativistic treatments [85]. This has been met by rapid rebuttals emphasizing that either the proposed model does, in fact, *not*, generate entanglement as claimed, or that any entanglement would, in this case, be mediated by quantized matter interactions rather than by a classical gravitational field [86,87]. Di Biagio has further contributed by isolating which assumptions in LOCC–like theorems are essential and how classical gravity can entangle once one relaxes particular constraints [88].

With this knowledge, the goal of the present chapter is more specific. Rather than comparing different candidate theories of gravity, we examine how far classical and quantum dynamics coincide when both are expressed in a shared language, and where they first diverge for the kinds of initial states and potentials used in the GME setups. In particular, we will compare the classical von Neumann evolution (CvN) to the standard quantum von Neumann (vN) evolution of Chapter 2 for an initially Gaussian two–body state, and we will show that the first quantifiable dynamical difference arises only once the gravitational potential is expanded beyond quadratic order. This will be precisely the regime in which non–Gaussianity and operator positivity issues become unavoidable. This connects directly to the broader theme developed earlier in this thesis, where we have shown that covariance–based witnesses are complete only in the Gaussian regime, while moving beyond it requires tracking positivity and genuinely nonclassical resources.

4.2. The setup

To quickly recap, the goal of GME–type setups is to put two masses into a spatial superposition of different branches. These branches then, in turn, accumulate different interaction phases, which can correlate and entangle the masses/spins. It is important to note here, that we do *not* consider (or try to prove) the "*entanglement implies quantum gravity*" claim, but instead we compare two dynamical maps, which give the same effective interaction model, and ask where they first diverge.

To obtain this effective description, it is instructive to see which approximations are typically used in these tabletop setups:

- Weak field: $Gm/(rc^2) \ll 1$.
- Nonrelativistic motion: $v/c \ll 1$.
- Near-field/quasistatic regime: interaction time T is much larger than the light crossing time L/c.
- Small superposition compared to separation: $r/L \ll 1$.

These approximations warrant the use of the Newtonian potential, which is not assumed as a fundamental nonlocal interaction, but as the leading-order effective description obtained from a causal, locally mediated field interaction in the near field and slow motion regime [72].

The following calculation starts out by clearly defining the initial states of a typical GME setup, as well as the Hamiltonian governing the total system. Then we redefine both the classical and the quantum von Neumann equations and proceed by expanding the Newtonian potential in the displacement–to–separation ratio r/L. We show that the typically used second–order truncation of the potential does not allow us to distinguish classical from quantum evolution. Only when going to third order, do we obtain quantifiable differences. Since the differential equations are no longer solvable analytically at third order, we will outline a split–step Fourier propagation method [89] to calculate the final states.

Both the initial state and the expansion of the gravitational potential are based on Kumar et al. [73]. We consider two particles with equal mass m located at positions x_A/x_B, with initial momentum p_0. The initial state of the composite system is then built out of the product of the two single particle wavefunctions, which are given by

$$\psi_A(x_A) = \left(\frac{1}{2\pi\sigma^2}\right)^{1/4} \exp\left(-\frac{x_A^2}{4\sigma^2} + i\frac{p_0}{\hbar}x_A\right), \tag{4.1}$$

$$\psi_B(x_B) = \left(\frac{1}{2\pi\sigma^2}\right)^{1/4} \exp\left(-\frac{x_B^2}{4\sigma^2} + i\frac{p_0}{\hbar}x_B\right) \tag{4.2}$$

and are governed by the non–relativistic Hamiltonian

$$\hat{H} = \frac{\hat{p}_A^2}{2m} + \frac{\hat{p}_B^2}{2m} - \frac{Gm^2}{L + (\hat{x}_B - \hat{x}_A)}. \tag{4.3}$$

To solve this system, it is beneficial to consider the center of mass (COM) frame, in which our state can be expressed as a product of a COM state $\phi(R, t = 0)$ and a relative coordinate state $\psi(r, t = 0)$, where $R = (x_A + x_B)/2$ and $r = x_B - x_A$. Since we want to consider the dynamics of the system, we can then drop the COM part of the wavefunction, as it would only undergo free evolution (see Appendix B.1 for a more detailed calculation). Finally, we obtain the CvN equation for the relative coordinates in matrix elements

$$i\hbar\partial_t\rho(r_x, r_y, t) = -\frac{\hbar^2}{m}(\partial_{r_x}^2 - \partial_{r_y}^2)\rho(r_x, r_y, t) + (r_x - r_y)V'\left(\frac{r_x + r_y}{2}\right)\rho(r_x, r_y, t), \tag{4.4}$$

whose form is similar to the quantum counterpart

$$i\hbar\partial_t\rho(r_x, r_y, t) = -\frac{\hbar^2}{m}(\partial_{r_x}^2 - \partial_{r_y}^2)\rho(r_x, r_y, t) + (V(r_x) - V(r_y))\rho(r_x, r_y, t). \tag{4.5}$$

In fact, these equations are identical, if potentials up to second order are considered [7]. This can easily be seen by considering a potential of the form $V(x) = a+bx+cx^2$ and plugging in the above potential terms

$$(r_x - r_y)V'\left(\frac{r_x + r_y}{2}\right) = (r_x - r_y)(b + c(r_x + r_y)) = b(r_x - r_y) + c(r_x^2 - r_y^2), \tag{4.6}$$

$$V(r_x) - V(r_y) = b(r_x - r_y) + c(r_x^2 - r_y^2). \tag{4.7}$$

In the gravitational context, this is indeed significant, as we have to take the expansion of the potential around the relative displacement at least to third order to obtain any differences in evolution at all. Using the characteristic frequency $\omega^2 = 4Gm/L^3$, where L denotes the initial separation of the particles, the expansion in the displacement–to–separation ratio r/L is defined as

$$V(r) = -\frac{1}{4}m\omega^2\left(L^2 - Lr + r^2 - \frac{r^3}{L} + \mathcal{O}(r^4)\right). \tag{4.8}$$

With the CvN equation of the relative coordinate density matrix in hand, we can now analytically compute the free evolution of the COM (see Appendix B.1) coordinate density matrix and compute the joint covariance matrix in lab coordinates (i.e., x_A, x_B), to apply the previously used covariance diagnostics.

4.3. Evolution and covariance

The classical evolution of the classical relative coordinate density matrix is performed via the split–step Fourier propagation method [90]. This method is typically useful for any Hamiltonians of the form $H = T + V$ and relies on propagation via small time increments. At each time step half of the potential is applied, after which a Fourier transformation is taken and the kinetic term $T = (\hbar/m)(k_x^2 - k_y^2)$ is applied. Finally, we take the inverse Fourier transform and apply the other half of the potential. One propagation step would then look like

$$\rho\left(t+\Delta t\right) = e^{-\frac{i}{2\hbar}\Delta t V_{\mathrm{cl}}}\mathcal{F}^{-1}\left[e^{-\frac{i}{\hbar}\Delta t T(k_x,k_y)}\mathcal{F}\left(e^{-\frac{i}{2\hbar}\Delta t V_{\mathrm{cl}}}\rho(t)\right)\right], \tag{4.9}$$

where V_{cl} is the classical potential term of Eq. (4.4). This allows us to efficiently propagate the relative coordinate density matrix forward in time. The full code for this procedure can be found in Appendix B.1, in particular code block B.1.

The evolution of the COM–coordinate moments can be computed analytically (see Appendix B.1 in Ref. [91]) and gives

$$\langle \hat{R} \rangle = 0, \tag{4.10}$$

$$\langle \hat{P} \rangle = 0, \tag{4.11}$$

$$\langle \hat{R}\hat{P} + \hat{P}\hat{R} \rangle = \hbar\omega_0 t, \tag{4.12}$$

$$\langle \hat{R}^2 \rangle = \frac{1}{2}\sigma^2(1+\omega_0^2 t^2), \tag{4.13}$$

$$\langle \hat{P}^2 \rangle = \frac{\hbar^2}{2\sigma^2}. \tag{4.14}$$

Furthermore, Ref. [91] shows how the covariance in lab coordinates $\Sigma_{ij} = \frac{1}{2}\langle\{\hat{z}_i, \hat{z}_j\}\rangle - \langle\hat{z}_i\rangle\langle\hat{z}_j\rangle$ can be constructed by the COM–relative coordinate moments, where $\hat{z} = (\hat{x}_A, \hat{p}_A, \hat{x}_B, \hat{p}_B)$ denotes the used quadrature vector. The final matrix elements are then given by

$$\Sigma_{00}\left(\Sigma_{02}\right) = \Delta R^2 + (-)\frac{1}{4}\Delta r^2, \tag{4.15}$$

$$\Sigma_{11}(\Sigma_{13}) = \frac{1}{4}\Delta P^2 + (-)\Delta p^2, \tag{4.16}$$

$$\Sigma_{01}(\Sigma_{03}) = \frac{1}{2}\mathrm{Cov}(R,P) + (-)\frac{1}{2}\mathrm{Cov}(r,p), \tag{4.17}$$

where the symmetry of the problem fixes $\Sigma_{22} = \Sigma_{00}$, $\Sigma_{33} = \Sigma_{11}$, $\Sigma_{23} = \Sigma_{01}$, $\Sigma_{12} = \Sigma_{03}$, while the rest is fixed by the symmetry of the covariance matrix itself. Now that we can compute the time evolution of the whole covariance matrix, we can apply the Positive Partial Transpose (PPT) and the Robertson–Schrödinger (RS) condition at a later time, to see whether *representational entanglement* emerges for a classical evolution of initial mass states.

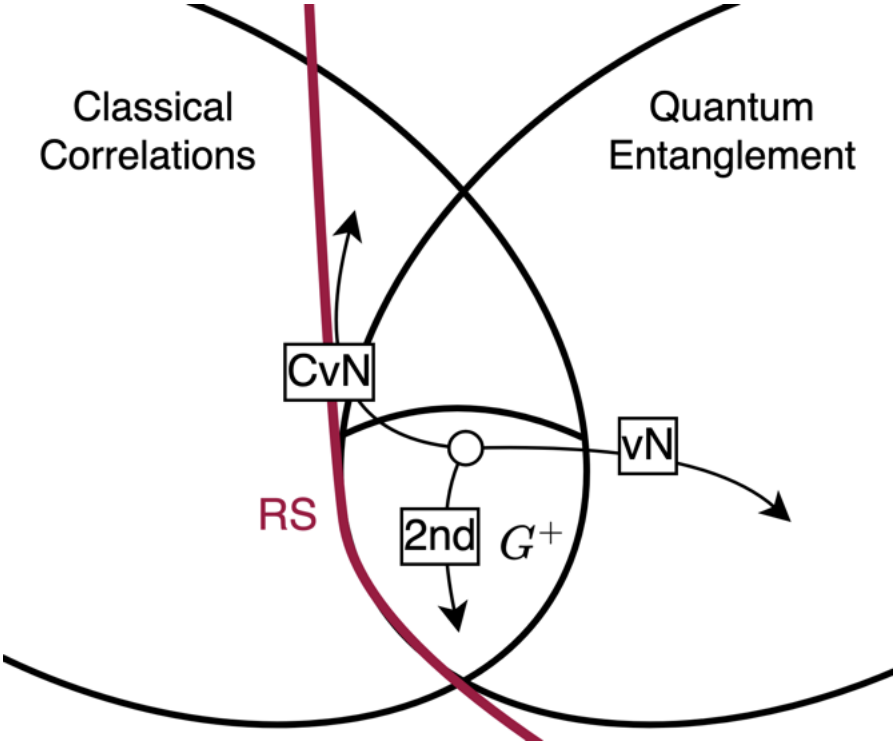

Figure 4.1.: Schematic sketch of where the initial state within G^+ evolves to for a second order truncation (2nd), a third order truncation of the classical von Neumann equation (CvN) and a third order truncation of the von Neumann equation (vN). Note that the respective transitions to the classical/quantum state space should, in theory, happen immediately.

4.4. Results

In this section, we compare CvN and vN time evolution for typically used initial states in gravity–mediated entanglement protocols. We show (i) that truncation of the Newtonian potential at second order yields identical dynamics and produces entanglement within the classical–quantum overlap $\mathcal{C} \cap \mathcal{Q}$ (HE in Sec. 3.4), (ii) the inclusion of third–order terms makes the quantum evolution immediately generate Wigner function negativity (GE in Sec. 3.5), while the classical evolution, on the other hand, drives the Hilbert space operator non–positive (RE in Sec. 3.3), and (iii) that despite these conceptual differences, the two final operators can remain extremely close in trace distance. Figures 4.1, 4.2 and 4.3 summarize these three points. Notice, however, that for a truncation of the potential at third order, requires numerical propagation, as described above. Details for this process can be found in Appendix B.

As we have seen in the previous section, a truncation of the Newtonian potential at

second order will leave the two evolutions indistinguishable and in fact, completely identical. This means that the initial Gaussian states in the G^+ set are mapped to an entangled state within the G^+ set. In the language of Chapter 3, this represents an instance of *hybrid entanglement*, i.e., entanglement within the $\mathcal{C} \cap \mathcal{Q}$ overlap, which is operationally compatible with a classical phase–space description. This can also be seen schematically in Fig. 4.1, where both the CvN and the regular vN evolution, when truncated at second order, coincide and stay within the G^+ set. *Therefore, to distinguish classical and quantum evolution, our experiment has to be sensitive to the third order in the gravitational potential.*

At third order, we would expect the quantum evolution to drive the initial state over into the quantum set and create a true entangled state, which would imply emerging negativity in the Wigner function. The simulation (see negativity volume in Appendix B.2) data confirms this and finds negativity in the Wigner function already at rather short times. To independently verify this, however, we can simply check how the Wigner function evolves according to Eq. (2.42) when the potential is truncated at third order. Defining $\mu = m/2$ and plugging in the potential of Eq. (4.8) then gives

$$\partial_t W = -\frac{p}{\mu}\partial_r W + V'(r)\partial_p W - \frac{\hbar^2 m\omega^2}{16L}\partial_p^3 W + \mathcal{O}(\hbar^4). \tag{4.18}$$

To demonstrate the onset of negativity, we choose an initially nonnegative Wigner function, e.g. a Gaussian in momentum,

$$W_0(r,p) = A(r)\exp\left[-\frac{(p-p_0)^2}{2\sigma_p^2}\right], \qquad A(r) > 0. \tag{4.19}$$

With $u := p - p_0$, one finds

$$\partial_p^3 W_0(r,p) = -\left(\frac{u^3}{\sigma_p^6} - \frac{3u}{\sigma_p^4}\right) W_0(r,p). \tag{4.20}$$

For short times,

$$W(r,p,t) = W_0(r,p) + t\,\partial_t W_0(r,p) + \mathcal{O}(t^2). \tag{4.21}$$

Keeping only the third-order contribution from Eq. (4.18) (and suppressing classical transport terms) gives

$$W(r,p,t) \approx W_0(r,p)\left[1 + t\,\frac{\hbar^2 m\omega^2}{16L}\left(\frac{u^3}{\sigma_p^6} - \frac{3u}{\sigma_p^4}\right)\right]. \tag{4.22}$$

Since $W_0(r,p) > 0$, the sign is determined by the bracket. The cubic polynomial in u is unbounded and tends to $-\infty$ for $u \to -\infty$, so for any fixed $t > 0$ there exist

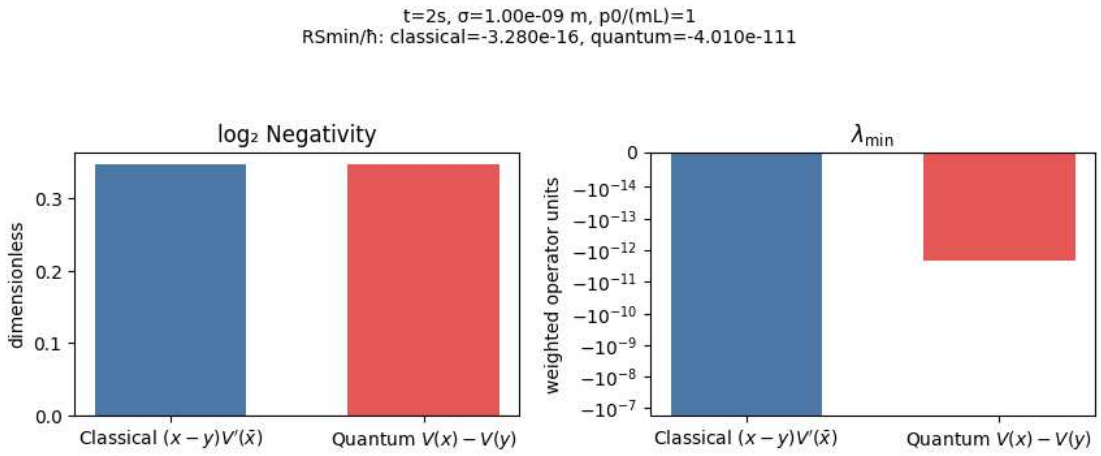

Figure 4.2.: Comparison of the final states of an evolution under the gravitational potential of Eq. 4.8 truncated at third order. The plot on the left–hand side shows the logarithmic negativity of both final states, while the plot on the right–hand side shows the operator eigenvalue of the (pseudo–) density operator. The classical evolution drives the classical density operator negative. The system was evolved for $t = 2$ s, with $\sigma = 1$ nm and $p_0/mL = 1$.

sufficiently negative u such that

$$1 + t\,\frac{\hbar^2 m\omega^2}{16L}\,\frac{u^3}{\sigma_p^6} < 0 \quad \Longrightarrow \quad u < -\left(\frac{16L\,\sigma_p^6}{t\,\hbar^2 m\omega^2}\right)^{1/3}. \tag{4.23}$$

Hence $W(r,p,t) < 0$ at some phase space points as soon as the third-order term is included. In this short-time, first-order expansion, the third-order quantum correction is therefore sufficient to induce Wigner-function negativity.

Figure 4.2 compares two diagnostics at $t = 2\,\mathrm{s}$: the logarithmic negativity (left) and the minimum eigenvalue of the evolved operator (right). Both CvN and vN generate comparable entanglement gain, as quantified by log-negativity. However, their positivity properties differ sharply: the CvN-evolved (pseudo-)density operator develops negative eigenvalues, whereas the vN-evolved density operator remains positive semidefinite. Importantly, the numerical values used in these simulations (mass, frequency, coupling scale, and evolution time) are chosen within the experimentally motivated orders of magnitude reported in the literature for near-term optomechanical [73], so the effect is not tied to unrealistic parameter choices. In the language of Chapter 3, this indicates that classical evolution can dynamically produce operators that fall outside the quantum set $\mathcal{Q}$, even though they may still reproduce certain phase space statistics. This motivates interpreting the CvN negativity as a dynamical route toward representational entanglement.

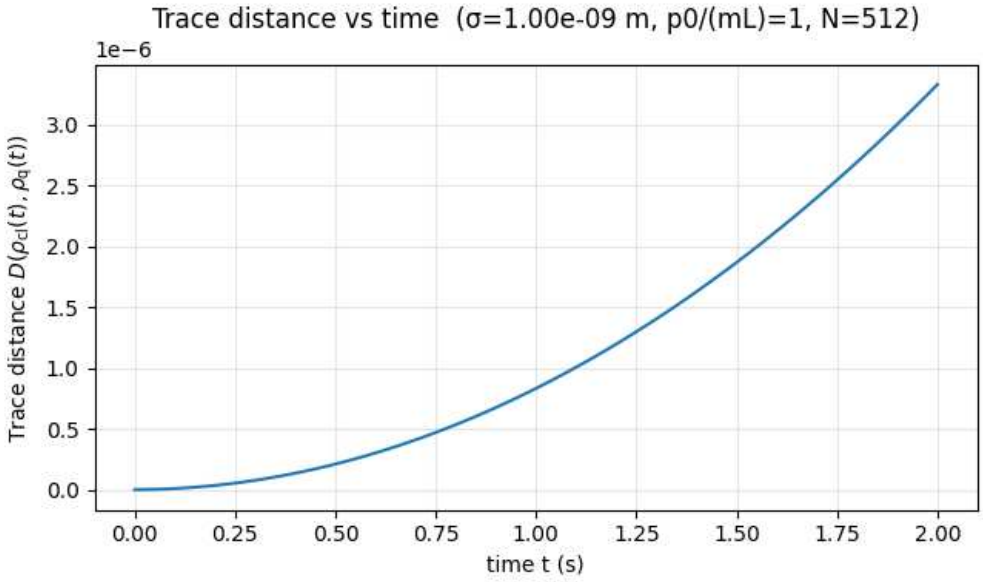

Figure 4.3.: Trace distance between the classical and quantum evolution of the initial density matrix under a truncation of the potential at third order. The evolution lasted $t = 2$ s, with $\sigma = 1$ nm and $p_0/mL = 1$.

While Figs. 4.2 and 4.1 would suggest that, upon including third–order effects of the potential, the final states become distinguishable, this is not necessarily the case. In particular, if we look at the trace distance between the two final states, we find that they are extremely similar (see Fig. 4.3), with trace distances of the order of 10^{-6}.

This means that even if it was experimentally feasible to detect third–order effects of the gravitational potential (e.g., by pushing the masses towards each other [73]), there remains the challenge of distinguishing a truly quantum evolution from its classical counterpart. Whether a distinction can be made in practice, either via a check of Wigner negativity or checking whether the resulting density matrix is positive semidefinite, remains an open question. In any case, regardless of what experimental platform might be suggested for the witnessing of GME effects, one needs to make sure that effects go beyond Gaussian evolution, to properly distinguish the predictions of the two theories.

4.5. Discussion

Chapter 3 distinguished three regimes of nonseparability: representational entanglement (RE), hybrid entanglement (HE), and genuine entanglement (GE).

In this chapter, we have applied these concepts to the GME framework and explicitly tracked the dynamical transitions between the corresponding nonseparability regimes. Second–order truncation produces entanglement while remaining in $G^+ \subseteq \mathcal{C} \cap \mathcal{Q}$, hence in the HE regime. At third order, the quantum evolution generates Wigner negativity, which is sufficient to leave $\mathcal{C}$ and this move toward the genuinely quantum set (GE). In contrast, the third–order classical evolution drives the Hilbert space operator non–positive, signaling a transition towards the RE–type behaviour discussed in Chapter 3. Since many practical implementations of this experiment rely on these covariance–based criteria, it is of great importance to exclude classical explanations stemming from within the RE/HE regime, before making any claims about the "quantumness" of the mediator.

The broader GME literature outlined above typically asks which classes of "classical" models are excluded by observed entanglement. Our analysis addresses a different issue: even within a shared language, classical and quantum dynamics can agree up to second order while still generating entanglement signatures at the covariance level. Therefore, covariance–based entanglement alone does not automatically imply a genuinely quantum mediator. To avoid these problems, one needs observables sensitive to the departure from the $\mathcal{C} \cap \mathcal{Q}$ overlap, such as Wigner negativity or other non–Gaussian features.

Two limitations stand out. First, the analytic result shows that Wigner negativity appears somewhere for arbitrarily small $t > 0$ once third–order terms are included, but the trace distance indicates that for the present parameters, the overall distinguishability can remain minimal. Second, numerical evolution requires careful consistency checks; in our implementation, the RS condition violations are negligible and likely numerical artifacts, and the Wigner negativity is confirmed by a finite negativity volume (Appendix B.2). A natural next step is therefore a parameter sweep (e.g., in σ, t and p_0/mL) to analyze in which regime an experimental distinction between the two evolutions might be possible.

5. General Conclusion

This thesis pursued a single guiding question from two complementary directions: under which operational conditions can entanglement-like signatures be reproduced classically, and where does a genuinely quantum boundary become unavoidable? The two main results answer this question at different layers. Firstly, we established an operational hierarchy of nonseparability in a unified phase space/Hilbert space representation. Secondly, we applied this perspective to gravity-mediated entanglement (GME) dynamics, showing how agreement at low order can break at higher order in the potential and drive the evolution beyond the classically reproducible regime.

The first result is conceptual and structural. By comparing classical and quantum descriptions within the same Wigner–Weyl framework, we showed that covariance-level signatures alone do not isolate genuine quantumness. This leads to a three-layer hierarchy: representational entanglement (RE), where nonseparability appears in Hilbert space representation without operator positivity; hybrid entanglement (HE), where states are positive and nonseparable but still admit a classical phase space model; and genuine entanglement (GE), where positivity is retained but classical reproducibility is excluded by nonclassicality criteria such as Wigner-function negativity. In this sense, the thesis clarifies that entanglement claims are not binary, as their interpretation depends on which operational constraints are imposed and which physicality conditions are verified.

The second result is dynamical. In the GME setting, classical and quantum evolutions can coincide up to second order while still producing covariance-level nonseparability signatures. At third order, however, quantum corrections become decisive, because the additional term can induce Wigner-function negativity and thus move the state out of the classical overlap. Numerically, this is mirrored by a sharp contrast between the classical von Neumann (CvN) and the quantum von Neumann (vN) evolved operators, where both can show comparable logarithmic-negativity gain, yet only the vN-evolved density operator remains positive semidefinite, whereas the CvN-evolved operator can develop negative eigenvalues. This distinction is central for GME interpretations, because covariance witnesses alone may overstate what has been established about the nature of the mediator.

Taken together, these two parts support a common message. First, a shared representation helps comparison, but only explicit positivity and nonclassicality tests determine whether certain features are genuinely quantum. Second, covariance-

based diagnostics are informative but incomplete outside the strictly Gaussian regime. Third, in GME-motivated scenarios, higher-order dynamics and positivity checks are not technical details; they are part of the physical conclusion. More concretely, observing covariance-level entanglement signatures is compatible with multiple interpretational layers (RE/HE/GE), and only additional operational tests can distinguish them.

The broader implication is methodological. Rather than treating the classical–quantum boundary as a single criterion, it is more precise to view it as a nested structure of admissible descriptions. Within this structure, representational artifacts, classically reproducible nonseparability, and genuinely quantum correlations can be cleanly separated. This provides a transparent framework for future analyses of GME proposals and continuous-variable experiments, where one should combine covariance witnesses with operator-positivity validation and, when possible, nonclassicality tests beyond second moments. In this way, the present work contributes both a conceptual map and practical criteria for identifying when entanglement signatures truly certify quantum behavior.

Bibliography

[1] Flavio Del Santo and Nicolas Gisin. Which features of quantum physics are not fundamentally quantum but are due to indeterminism? *Quantum*, 9:1686, April 2025. arXiv:2409.10601 [quant-ph].

[2] Albert Einstein. Über die entwicklung unserer anschauungen über das wesen und die konstitution der strahlung. *Physikalische Blätter*, 25(9):386–391, 1969.

[3] W. E. Lamb and M. O. Scully. The photoelectric effect without photons. Technical Report TS-QED-68-1, February 1968. NTRS Author Affiliations: Miami Univ. NTRS Document ID: 19680009569 NTRS Research Center: Legacy CDMS (CDMS).

[4] Stuart J. Freedman and John F. Clauser. Experimental Test of Local Hidden-Variable Theories. *Physical Review Letters*, 28(14):938–941, April 1972.

[5] Samuel Schlegel, Borivoje Dakić, and Flavio Del Santo. Entanglement without Quantum Mechanics: Operational Constraints on the Quantum Signature, December 2025. arXiv:2512.14834 [quant-ph].

[6] Herbert Goldstein, Charles P. Poole Jr, and John L. Safko Sr. *Klassische Mechanik*. John Wiley & Sons, April 2012. Google-Books-ID: z_zmcPqMKMYC.

[7] D. Bohm and B. J. Hiley. On a quantum algebraic approach to a generalized phase space. *Foundations of Physics*, 11(3):179–203, April 1981.

[8] D. Mauro. Topics in Koopman-von Neumann Theory, January 2003. arXiv:quant-ph/0301172.

[9] Ideal Majtara. Classical-Quantum dualities. February 2025. Accepted: 2022-04-08T10:46:18Z.

[10] H. Weyl. Quantenmechanik und Gruppentheorie. *Zeitschrift für Physik*, 46(1):1–46, November 1927.

[11] Andrea Carosso. Quantization: History and Problems, February 2022. arXiv:2202.07838 [physics].

[12] Hilbrand Johannes Groenewold. On the Principles of Elementary Quantum Mechanics. In Hilbrand Johannes Groenewold, editor, *On the Principles of Elementary Quantum Mechanics*, pages 1–56. Springer Netherlands, Dordrecht, 1946.

[13] Léon Van Hove. Sur le problème des relations entre les transformations unitaires de la Mécanique quantique et les transformations canoniques de la Mécanique classique. *Bulletins de l'Académie Royale de Belgique*, 37(1):610–620, 1951.

[14] J. E. Moyal. Quantum mechanics as a statistical theory. *Mathematical Proceedings of the Cambridge Philosophical Society*, 45(1):99–124, January 1949.

[15] J. v. Neumann. Zur Operatorenmethode In Der Klassischen Mechanik. *Annals of Mathematics*, 33(3):587–642, 1932.

[16] Michael A. Nielsen and Isaac L. Chuang. *Quantum Computation and Quantum Information: 10th Anniversary Edition*. Cambridge University Press, December 2010.

[17] J. J. Sakurai and Jim Napolitano. *Modern Quantum Mechanics*. Cambridge University Press, September 2020. Google-Books-ID: sUUBEAAAQBAJ.

[18] Gerhart Lüders. Über die Zustandsänderung durch den Meßprozeß. *Annalen der Physik*, 443(5-8):322–328, 1950.

[19] The Measuring Process. In Asher Peres, editor, *Quantum Theory: Concepts and Methods*, pages 373–429. Springer Netherlands, Dordrecht, 2002.

[20] Paul Busch, Pekka J. Lathi, and Peter Mittelstaedt. *The Quantum Theory of Measurement*. Lecture Notes in Physics Monographs. Springer, Berlin, Heidelberg, 1996.

[21] Ryszard Horodecki, Paweł Horodecki, Michał Horodecki, and Karol Horodecki. Quantum entanglement. *Reviews of Modern Physics*, 81(2):865–942, June 2009.

[22] Thomas L. Curtright, David B. Fairlie, and Cosmas K. Zachos. *A Concise Treatise On Quantum Mechanics In Phase Space*. World Scientific Publishing Company, November 2013. Google-Books-ID: WSs8DQAAQBAJ.

[23] M. Hillery, R. F. O'Connell, M. O. Scully, and E. P. Wigner. Distribution functions in physics: Fundamentals. *Physics Reports*, 106(3):121–167, April 1984.

[24] E. Wigner. On the Quantum Correction For Thermodynamic Equilibrium. *Physical Review*, 40(5):749–759, June 1932.

[25] K. E. Cahill and R. J. Glauber. Ordered Expansions in Boson Amplitude Operators. *Physical Review*, 177(5):1857–1881, January 1969.

[26] Anatoli Polkovnikov. Phase space representation of quantum dynamics. *Annals of Physics*, 325(8):1790–1852, August 2010. arXiv:0905.3384 [cond-mat].

[27] Christopher Ferrie. Quasi-probability representations of quantum theory with applications to quantum information science. *Reports on Progress in Physics*, 74(11):116001, October 2011.

[28] Eric J. Heller. Wigner phase space method: Analysis for semiclassical applications. *The Journal of Chemical Physics*, 65(4):1289–1298, August 1976.

[29] Jian Liu and William H. Miller. Linearized semiclassical initial value time correlation functions using the thermal Gaussian approximation: Applications to condensed phase systems. *The Journal of Chemical Physics*, 127(11):114506, September 2007.

[30] William H. Miller. Perspective: Quantum or classical coherence? *The Journal of Chemical Physics*, 136(21):210901, June 2012.

[31] A. Isar, A. Sandulescu, H. Scutaru, E. Stefanescu, and W. Scheid. Open quantum systems. *International Journal of Modern Physics E*, 03(02):635–714, June 1994.

[32] K. Vogel and H. Risken. Determination of quasiprobability distributions in terms of probability distributions for the rotated quadrature phase. *Physical Review A*, 40(5):2847–2849, September 1989.

[33] R. Simon. Peres-Horodecki separability criterion for continuous variable systems. *Physical Review Letters*, 84(12):2726–2729, March 2000. arXiv:quant-ph/9909044.

[34] Lu-Ming Duan, G. Giedke, J. I. Cirac, and P. Zoller. Inseparability Criterion for Continuous Variable Systems. *Physical Review Letters*, 84(12):2722–2725, March 2000.

[35] G. Vidal and R. F. Werner. Computable measure of entanglement. *Physical Review A*, 65(3):032314, February 2002.

[36] Christian Weedbrook, Stefano Pirandola, Raul Garcia-Patron, Nicolas J. Cerf, Timothy C. Ralph, Jeffrey H. Shapiro, and Seth Lloyd. Gaussian Quantum Information. *Reviews of Modern Physics*, 84(2):621–669, May 2012. arXiv:1110.3234 [quant-ph].

[37] Alessio Serafini. *Quantum Continuous Variables: A Primer of Theoretical Methods*. CRC Press, Boca Raton, 2 edition, August 2023.

[38] R. F. Werner and M. M. Wolf. Bound entangled Gaussian states. *Physical Review Letters*, 86(16):3658–3661, April 2001. arXiv:quant-ph/0009118.

[39] Roy J Glauber. Coherent and incoherent states of the radiation field. *Physical Review*, 131(6):2766, 1963.

[40] Leonard Mandel and Emil Wolf. *Optical Coherence and Quantum Optics*. Cambridge University Press, September 1995. Google-Books-ID: FeBix14iM70C.

[41] Anatole Kenfack and Karol Zyczkowski. Negativity of the Wigner function as an indicator of nonclassicality. *Journal of Optics B: Quantum and Semiclassical Optics*, 6(10):396–404, October 2004. arXiv:quant-ph/0406015.

[42] Th. Richter and W. Vogel. Nonclassicality of Quantum States: A Hierarchy of Observable Conditions. *Physical Review Letters*, 89(28):283601, December 2002.

[43] Robert W. Spekkens. In defense of the epistemic view of quantum states: a toy theory. *Physical Review A*, 75(3):032110, March 2007. arXiv:quant-ph/0401052.

[44] Lorenzo Catani, Matthew Leifer, Giovanni Scala, David Schmid, and Robert W. Spekkens. What is nonclassical about uncertainty relations? *Physical Review Letters*, 129(24):240401, December 2022. arXiv:2207.11779 [quant-ph].

[45] Lorenzo Catani, Matthew Leifer, David Schmid, and Robert W. Spekkens. Why interference phenomena do not capture the essence of quantum theory. *Quantum*, 7:1119, September 2023. arXiv:2111.13727 [quant-ph].

[46] Lorenzo Catani, Matthew Leifer, Giovanni Scala, David Schmid, and Robert W. Spekkens. Aspects of the phenomenology of interference that are genuinely nonclassical. *Physical Review A*, 108(2):022207, August 2023. arXiv:2211.09850 [quant-ph].

[47] Johannes Fankhauser, Tomáš Gonda, and Gemma De les Coves. Epistemic Horizons From Deterministic Laws: Lessons From a Nomic Toy Theory. *Synthese*, 205(4):136, March 2025. arXiv:2406.17581 [quant-ph].

[48] Flavio Del Santo and Nicolas Gisin. Physics without Determinism: Alternative Interpretations of Classical Physics. *Physical Review A*, 100(6):062107, December 2019. arXiv:1909.03697 [quant-ph].

[49] Giulio Chiribella, Lorenzo Giannelli, and Carlo Maria Scandolo. Bell Nonlocality in Classical Systems Coexisting with Other System Types. *Physical Review Letters*, 132(19):190201, May 2024.

[50] Giacomo Mauro D'Ariano, Marco Erba, and Paolo Perinotti. Classical theories with entanglement. *Physical Review A*, 101(4):042118, April 2020.

[51] Robert J. C. Spreeuw. A Classical Analogy of Entanglement. *Foundations of Physics*, 28(3):361–374, March 1998.

[52] Andrew Forbes, Andrea Aiello, and Bienvenu Ndagano. Chapter Three - Classically Entangled Light. In Taco D. Visser, editor, *Progress in Optics*, volume 64, pages 99–153. Elsevier, January 2019.

[53] Ebrahim Karimi and Robert W. Boyd. Classical entanglement? *Science*, 350(6265):1172–1173, December 2015.

[54] Natalia Korolkova, Luis Sánchez-Soto, and Gerd Leuchs. An operational distinction between quantum entanglement and classical non-separability. *Philosophical Transactions of the Royal Society A: Mathematical, Physical and Engineering Sciences*, 382(2287):20230342, December 2024.

[55] Semiclassical Methods. In Asher Peres, editor, *Quantum Theory: Concepts and Methods*, pages 298–331. Springer Netherlands, Dordrecht, 2002.

[56] Christopher C. Gerry and Peter L. Knight. *Introductory Quantum Optics*. Cambridge University Press, November 2023.

[57] Gerardo Adesso and Fabrizio Illuminati. Entanglement in continuous variable systems: Recent advances and current perspectives. *Journal of Physics A: Mathematical and Theoretical*, 40(28):7821–7880, July 2007. arXiv:quant-ph/0701221.

[58] Ruslan Leont'evich Stratonovich. On distributions in representation space. *Soviet Physics JETP-USSR*, 4(6):891–898, 1957.

[59] C. F. Ockeloen-Korppi, E. Damskägg, J.-M. Pirkkalainen, M. Asjad, A. A. Clerk, F. Massel, M. J. Woolley, and M. A. Sillanpää. Stabilized entanglement of massive mechanical oscillators. *Nature*, 556(7702):478–482, April 2018.

[60] Markus Aspelmeyer, Tobias J. Kippenberg, and Florian Marquardt. Cavity optomechanics. *Reviews of Modern Physics*, 86(4):1391–1452, December 2014.

[61] Alessandro Ferraro, Stefano Olivares, and Matteo G. A. Paris. Gaussian states in continuous variable quantum information, March 2005. arXiv:quant-ph/0503237.

[62] Daniel Collins and Sandu Popescu. Classical analog of entanglement. *Physical Review A*, 65(3):032321, February 2002.

[63] Alexei Ourjoumtsev, Rosa Tualle-Brouri, and Philippe Grangier. Quantum Homodyne Tomography of a Two-Photon Fock State. *Physical Review Letters*, 96(21):213601, June 2006.

[64] Stephen D. Bartlett, Terry Rudolph, and Robert W. Spekkens. Reconstruction of Gaussian quantum mechanics from Liouville mechanics with an epistemic restriction. *Physical Review A*, 86(1):012103, July 2012. arXiv:1111.5057 [quant-ph].

[65] R. L. Hudson. When is the wigner quasi-probability density non-negative? *Reports on Mathematical Physics*, 6(2):249–252, October 1974.

[66] A. Mandilara, E. Karpov, and N. J. Cerf. Extending Hudson's theorem to mixed quantum states. *Physical Review A*, 79(6):062302, June 2009.

[67] Maxime Oliva and Ole Steuernagel. Quantum Kerr oscillators' evolution in phase space: Wigner current, symmetries, shear suppression, and special states. *Physical Review A*, 99(3):032104, March 2019.

[68] R. M. Gomes, A. Salles, F. Toscano, P. H. Souto Ribeiro, and S. P. Walborn. Quantum entanglement beyond Gaussian criteria. *Proceedings of the National Academy of Sciences*, 106(51):21517–21520, December 2009.

[69] Anaelle Hertz, Evgueni Karpov, Aikaterini Mandilara, and Nicolas J. Cerf. Detection of non-Gaussian entangled states with an improved continuous-variable separability criterion. *Physical Review A*, 93(3):032330, March 2016. arXiv:1511.06621 [quant-ph].

[70] Sougato Bose, Anupam Mazumdar, Gavin W. Morley, Hendrik Ulbricht, Marko Toroš, Mauro Paternostro, Andrew Geraci, Peter Barker, M. S. Kim, and Gerard Milburn. A Spin Entanglement Witness for Quantum Gravity, July 2017. arXiv:1707.06050.

[71] Chiara Marletto and Vlatko Vedral. Gravitationally-induced entanglement between two massive particles is sufficient evidence of quantum effects in gravity, December 2017. arXiv:1707.06036.

[72] Marios Christodoulou, Andrea Di Biagio, Markus Aspelmeyer, Časlav Brukner, Carlo Rovelli, and Richard Howl. Locally mediated entanglement in linearised quantum gravity, December 2023. arXiv:2202.03368.

[73] Ankit Kumar, Tanjung Krisnanda, Paramasivan Arumugam, and Tomasz Paterek. Continuous-Variable Entanglement through Central Forces: Application to Gravity between Quantum Masses. *Quantum*, 7:1008, May 2023.

[74] Simone Rijavec, Matteo Carlesso, Angelo Bassi, Vlatko Vedral, and Chiara Marletto. Decoherence effects in non-classicality tests of gravity. *New Journal of Physics*, 23(4):043040, April 2021. arXiv:2012.06230 [quant-ph].

[75] Martine Schut, Alexey Grinin, Andrew Dana, Sougato Bose, Andrew Geraci, and Anupam Mazumdar. Relaxation of experimental parameters in a quantum-gravity-induced entanglement of masses protocol using electromagnetic screening. *Physical Review Research*, 5(4):043170, November 2023.

[76] Tanjung Krisnanda, Guo Yao Tham, Mauro Paternostro, and Tomasz Paterek. Observable quantum entanglement due to gravity, January 2020. arXiv:1906.08808.

[77] Akira Matsumura and Kazuhiro Yamamoto. Gravity-induced entanglement in optomechanical systems. *Physical Review D*, 102(10):106021, November 2020.

[78] Ofek Bengyat, Andrea Di Biagio, Markus Aspelmeyer, and Marios Christodoulou. Gravity Mediated Entanglement between Oscillators as Quantum Superposition of Geometries, September 2023. arXiv:2309.16312.

[79] D. Kafri, J. M. Taylor, and G. J. Milburn. A classical channel model for gravitational decoherence. *New Journal of Physics*, 16(6):065020, June 2014. arXiv:1401.0946 [quant-ph].

[80] Antoine Tilloy and Lajos Diósi. Sourcing semiclassical gravity from spontaneously localized quantum matter. *Physical Review D*, 93(2):024026, January 2016. arXiv:1509.08705 [quant-ph].

[81] Antoine Tilloy and Lajos Diósi. Principle of least decoherence for Newtonian semi-classical gravity. *Physical Review D*, 96(10):104045, November 2017. arXiv:1706.01856 [quant-ph].

[82] Antoine Tilloy. Does gravity have to be quantized? Lessons from non-relativistic toy models. *Journal of Physics: Conference Series*, 1275(1):012006, September 2019. arXiv:1903.01823 [quant-ph].

[83] Richard Howl, Vlatko Vedral, Devang Naik, Marios Christodoulou, Carlo Rovelli, and Aditya Iyer. Non-Gaussianity as a Signature of a Quantum Theory of Gravity. *PRX Quantum*, 2(1):010325, February 2021.

[84] Ludovico Lami, Julen S. Pedernales, and Martin B. Plenio. Testing the Quantumness of Gravity without Entanglement. *Physical Review X*, 14:021022, May 2024. ADS Bibcode: 2024PhRvX..14b1022L.

[85] Joseph Aziz and Richard Howl. Classical theories of gravity produce entanglement. *Nature*, 646(8086):813–817, October 2025.

[86] Lajos Diósi. No, classical gravity does not entangle quantized matter fields, November 2025. arXiv:2511.00852 [quant-ph].

[87] Chiara Marletto, Jonathan Oppenheim, Vlatko Vedral, and Elizabeth Wilson. Classical gravity cannot mediate entanglement, November 2025. arXiv:2511.07348 [quant-ph].

[88] Andrea Di Biagio. The simple reason why classical gravity can entangle, November 2025. arXiv:2511.02683 [gr-qc].

[89] JA Fleck Jr, JR Morris, and MD Feit. Time-dependent propagation of high energy laser beams through the atmosphere. *Applied physics*, 10(2):129–160, 1976.

[90] M. D Feit, J. A Fleck, and A Steiger. Solution of the Schrödinger equation by a spectral method. *Journal of Computational Physics*, 47(3):412–433, September 1982.

[91] Ankit Kumar. Entanglement Dynamics in Quantum Continuous-Variable States, May 2024. arXiv:2405.07362 [quant-ph].

A. Representational/Hybrid Entanglement

A.1. Displaced mixtures in Hilbert space & numerical diagonalization

To transform a mixture of two classical Gaussian distributions to Hilbert space and check their positivity, the calculation is easiest, when considering configuration space matrix elements. Recall the Weyl-transformation of classical phase space distributions in Eq. 3.1. The matrix element of the Weyl-kernel can be written as

$$\langle x|\,\hat{\Delta}(q,p)\,|x'\rangle = \int \frac{ds}{2\pi\hbar} e^{\frac{ips}{\hbar}}\,\langle x|q-s/2\rangle\,\langle q+s/2|x'\rangle\,, \tag{A.1}$$

giving us two δ-functions. One can be used to carry out the ds integration giving us

$$\langle x|\,\hat{\Delta}\,|x'\rangle = \frac{1}{2\pi\hbar} e^{2ip(q-x)/\hbar}\delta(x'+x-2q), \tag{A.2}$$

which can be used to carry out the dq integration of Eq. 3.1 to obtain the matrix element of the density matrix

$$\langle x|\,\hat{\rho}_{\rm cl}\,|x'\rangle = \frac{1}{2\pi\hbar}\int dp e^{ip(x'-x)} P\left(\frac{x+x'}{2},p\right), \tag{A.3}$$

where P denotes the phase space distribution. Note that we have successfully reduced the number of integrals from three, to just one. Now we can evaluate the single-mode Gaussian at $(x+y)/2$ and obtain

$$P\left(\frac{x+y}{2},p;d\right) = \frac{1}{2\pi\sigma_x\sigma_p}\exp\left[-\frac{(\frac{x+y}{2}-d)^2}{2\sigma_x^2}\right]\exp\left[-\frac{p^2}{2\sigma_p^2}\right]. \tag{A.4}$$

Now we can perform the Gaussian integral

$$\int dp e^{\frac{i}{\hbar}p(x-x')} e^{-\frac{p^2}{2\sigma_p^2}} = \sqrt{2\pi}\sigma_p \exp\left[-\frac{\sigma_p^2}{2\hbar^2}(x-x')^2\right] \tag{A.5}$$

and after collecting the prefactors, we obtain exactly the expression from Eq. 3.23

$$\rho(x,x') = \langle x|\,\hat{\rho}\,|x'\rangle = \frac{1}{(2\pi)^{3/2}\hbar\sigma_x}\exp\left[-\frac{(\frac{x+x'}{2}-d)^2}{2\sigma_x^2}\right]\exp\left[-\frac{\sigma_p^2}{2\hbar^2}(x-x')^2\right]. \tag{A.6}$$

Let us now proceed by discretizing Eq. 3.25 on the lattice and discussing the code in A.1. We fist define the parameters $\sigma_{xA}, \sigma_{pA}, \sigma_{xB}, \sigma_{pB}$ in units where $\hbar = 1$ and then proceed by defining the helper function *nu_A(d)* that calculates the smallest symplectic eigenvalue of mode A. The smallest symplectic eigenvalue is constant and can just be defined like the threshold value d_*. The function *rho_G_xy* then implements the closed-form position-basis matrix element we have just derived. Finally, we build the two mode operator with the function *build_two_mode_rho*. Here we choose the lattice size via $x_{\max}$, where we have to ensure that the Gaussians are sufficiently well contained on the lattice to avoid boundary errors. Furthermore, we normalize each kernel to trace 1 before tensoring to make sure that $\mathrm{Tr}\rho_{AB} = 1$ automatically (note that this makes our results insensitive to the chosen prefactor). Now the code simply iterates over these functions for different d values and records the minimum eigenvalue $\lambda_{\min}(d)$ and the smallest symplectic eigenvalue $\nu_{\min}(d)$. This procedure is exactly what was used for Fig. 3.4.

```python
import numpy as np
import matplotlib.pyplot as plt

hbar = 1.0
sigma_xA, sigma_pA = 0.6, 0.6
sigma_xB, sigma_pB = 1.0, 1.0

def nu_A(d):
    return sigma_pA * np.sqrt(sigma_xA**2 + d**2)

nu_B = sigma_xB * sigma_pB
RS_bound = hbar/2

def rho_G_xy(X, Y, d, sigma_x, sigma_p, hbar):
    mid  = 0.5*(X + Y)
    diff = (X - Y)
    pref = 1.0/(np.sqrt((2.0*np.pi)**3)*hbar*sigma_x)
    return pref * np.exp(-((mid - d)**2)/(2.0*sigma_x**2)) \
                * np.exp(-(sigma_p**2)*(diff**2)/(2.0*hbar**2))

def build_two_mode_rho(d, N=33, xmaxA=8.0, xmaxB=8.0):
    xA = np.linspace(-xmaxA, xmaxA, N)
    xB = np.linspace(-xmaxB, xmaxB, N)
    dxA = xA[1] - xA[0]
    dxB = xB[1] - xB[0]
    XA, YA = np.meshgrid(xA, xA, indexing='ij')
    XB, YB = np.meshgrid(xB, xB, indexing='ij')

    rhoA_plus  = rho_G_xy(XA, YA, +d, sigma_xA, sigma_pA, hbar)
    rhoA_minus = rho_G_xy(XA, YA, -d, sigma_xA, sigma_pA, hbar)
    rhoB       = rho_G_xy(XB, YB,  0.0, sigma_xB, sigma_pB, hbar)

    def tr1(rho, dx):
        return np.sum(np.real(np.diag(rho))) * dx
    rhoA_plus  /= tr1(rhoA_plus,  dxA)
    rhoA_minus /= tr1(rhoA_minus, dxA)
    rhoB       /= tr1(rhoB,       dxB)

    rhoAB_plus  = np.kron(rhoA_plus,  rhoB)
    rhoAB_minus = np.kron(rhoA_minus, rhoB)
    rhoAB = 0.5*(rhoAB_plus + rhoAB_minus)
    rhoAB = 0.5*(rhoAB + rhoAB.conj().T)
    return rhoAB
```

Listing A.1: Two-mode displaced-mixture diagonalization.

A.2. Symplectic eigenvalue conditions

For the required class of states in Ch. 3.3, we need to fulfill three things:

1. Σ_0 fails RS,
2. Σ passes RS,
3. Σ fails PPT.

According to theorem 2, for a state to fail (or pass) RS, the smallest symplectic eigenvalue has to be smaller (or bigger) than $\hbar/2$. Similarly, for PPT to fail, the smallest symplectic eigenvalue of the partially transposed matrix has to be smaller than $\hbar/2$. Since these are four by four matrices, this calculation could be done by hand, but is simple to implement in Python, as we can see in A.2, where the analytical expression for the symplectic eigenvalues is returned. Running this code for Σ_0 will yield the two distinct eigenvalues

$$\nu_1^0 = \nu_2^0 = \sqrt{k_p k_q + k_p s_q + k_q s_p + s_q s_p}, \tag{A.7}$$
$$\nu_3^0 = \nu_4^0 = \sqrt{k_p k_q - k_p s_q - k_q s_p + s_q s_p}. \tag{A.8}$$
$$\tag{A.9}$$

Since we have to take the minimal symplectic eigenvalue for our conditions and a sign switch of the k's changes it from one to the other, we can alternatively write the condition as

$$\nu_{\text{min}}^0 = \sqrt{k_p k_q + s_p s_q - |k_p s_q + k_q s_p|} < \frac{\hbar}{2}, \tag{A.10}$$

incorporating both cases by using the absolute value.

Similarly, the code in A.2 gives us the following eigenvalues for Σ

$$\nu_A = \nu_1 = \nu_2 = \sqrt{k_p k_q + k_p s_q + k_q s_p + s_p s_q}, \tag{A.11}$$
$$\nu_B = \nu_3 = \nu_4 = \sqrt{-2d^2 k_p + 2d^2 s_p + k_p k_q - k_p s_q - k_q s_p + s_q s_p}, \tag{A.12}$$

where we cannot immediately see which one is smaller. But we know that to compensate for the RS violation of Σ_0, we need to consider the d-dependent eigenvalue. To warrant this "choice," we have to ensure that $\nu_B(0) < \nu_A = const.$. Secondly, we do not want our constant eigenvalue ν_A to be under the RS threshold and have to enforce $\nu_A > \hbar/2$. Doing this allows us to write down the condition

$$\nu_B(d)^2 = (s_q - k_q + 2d^2)(s_p - k_p) \geq \left(\frac{\hbar}{2}\right)^2, \tag{A.13}$$

which can be reformulated to give us the threshold value

$$d_*^2 \geq \frac{1}{2}\left[\frac{(\hbar/2)^2}{s_p - k_p} - (s_q - k_q)\right]. \tag{A.14}$$

Note that we divided by $(s_p - k_p)$ and have to make sure that this is positive for the above inequality to hold. Lastly, we can compute the symplectic eigenvalues of the partially transposed covariance Σ^Γ to be

$$\tilde{\nu}_1 = \tilde{\nu}_2 = \sqrt{-k_p k_q - k_p s_q + k_q s_p + s_p s_q}, \tag{A.15}$$

$$\tilde{\nu}_3 = \tilde{\nu}_4 = \sqrt{2d^2 k_p + 2d^2 s_p - k_p k_q + k_p s_q - k_q s_p + s_p s_q}. \tag{A.16}$$

```python
from IPython.display import display, Math
import sympy as sp


def symplectic_eigenvalues_symbolic():
    s_q, s_p, d = sp.symbols('s_q s_p d ', real=True, positive=
    True)
    k_q, k_p = sp.symbols('k_q, k_p', real=True)

    M = sp.Matrix([
        [s_q, 0, k_q, 0],
        [0, s_p, 0, k_p],
        [k_q, 0, s_q, 0],
        [0, k_p, 0, s_p]
    ])
    display(Math(sp.latex(M)))
    J = sp.Matrix([[0, 1], [-1, 0]])
    Omega = sp.diag(J, J)

    eigvals = (sp.I * Omega * M).eigenvals()

    symplectic_eigs = [sp.simplify(abs(ev)) for ev in eigvals]

    return symplectic_eigs

symplectic_eigs = symplectic_eigenvalues_symbolic()

print("Symplectic eigenvalues:")
display(Math(sp.latex(symplectic_eigs)))
```

Listing A.2: Calculation of symplectic eigenvalues.

A.3. Derivation of the kernel formula

We begin from the general relation between a phase space probability distribution and the density matrix in the position basis (see Appendix A.1)

$$\langle x|\,\rho\,|y\rangle = \frac{1}{(2\pi\hbar)^2}\int d^2p P(m,p)e^{\frac{i}{\hbar}\Delta^T p}, \tag{A.17}$$

with $m = (x+y)/2$ and $\Delta = x - y$. For a Gaussian state with mean $\mu = (\bar{q},\bar{p})$ and covariance Σ_0, the probability distribution cam be written as

$$P(q,p) = \frac{1}{2\pi\sqrt{\det\Sigma_0}}\exp\left[-\frac{1}{2}(R-\mu)^T\Sigma_0^{-1}(R-\mu)\right], \quad R=(q,p), \tag{A.18}$$

where the quantities q and p now represent two dimensional vectors. Since the covariance matrix is block diagonal and of the form

$$\Sigma_0 = \begin{pmatrix} Q_0 & 0 \\ 0 & p_0 \end{pmatrix}, \tag{A.19}$$

we can pull out the position part of the integral and simplify to

$$\langle x|\,\rho\,|y\rangle = \frac{1}{(2\pi)^4\hbar^2\sqrt{\det Q_0 \det P_0}}\exp\left[-\frac{1}{2}(m-\bar{q})^T Q_0^{-1}(m-\bar{q})\right] I(\Delta). \tag{A.20}$$

The integral of the form

$$I(\Delta) = \int d^2p\,\exp\left[-\frac{1}{2}p^T P_0^{-1}p + \frac{i}{\hbar}\Delta^T p\right] \tag{A.21}$$

is of standard Gaussian form and can be computed to be

$$I(\Delta) = (2\pi)\sqrt{\det P_0}\exp\left[-\frac{1}{2\hbar^2}\Delta^T P_0\Delta\right], \tag{A.22}$$

making the final matrix element

$$K(x,y;\mu_\pm,\Sigma_0) = \frac{1}{(2\pi)^3\hbar^2\sqrt{\det Q_0}}\exp\left[-\frac{1}{2}(m-\bar{q}_\pm)^T Q_0^{-1}(m-\bar{q}_\pm)\right]\exp\left[-\frac{1}{2\hbar^2}\Delta^T P_0\Delta\right]. \tag{A.23}$$

A.4. Hybrid beamsplitter state

We start from the single-mode mixed state of Eq. 3.36,

$$\rho(p) = p\,|0\rangle\langle 0| + (1-p)\,|1\rangle\langle 1|\,, \quad 0 \leq p \leq 1, \tag{A.24}$$

and prepare a two mode input state

$$\rho_{\text{in}}(p) = \rho(p) \otimes |0\rangle\langle 0|\,, \tag{A.25}$$

where the second mode is in the vacuum. A balanced beamsplitter U_{BS} acts on the relevant Fock states as

$$U_{BS}\,|0,0\rangle = |0,0\rangle\,, \quad U_{BS}\,|1,0\rangle = |\psi_+\rangle := \frac{|1,0\rangle + |0,1\rangle}{\sqrt{2}}. \tag{A.26}$$

The output state in the Fock basis $\{|00\rangle, |01\rangle, |10\rangle, |11\rangle\}$, is therefore

$$\rho_{AB}(p) = \begin{pmatrix} p & 0 & 0 & 0 \\ 0 & \frac{1}{2}-\frac{p}{2} & \frac{1}{2}-\frac{p}{2} & 0 \\ 0 & \frac{1}{2}-\frac{p}{2} & \frac{1}{2}-\frac{p}{2} & 0 \\ 0 & 0 & 0 & 0 \end{pmatrix}. \tag{A.27}$$

Partial transposition with respect to subsystem B amounts to transposing the matrix elements that connect $|0,1\rangle$ and $|1,0\rangle$. This yields

$$\rho_{AB}^{PT}(p) = \begin{pmatrix} p & 0 & 0 & \frac{1}{2}-\frac{p}{2} \\ 0 & \frac{1}{2}-\frac{p}{2} & 0 & 0 \\ 0 & 0 & \frac{1}{2}-\frac{p}{2} & 0 \\ \frac{1}{2}-\frac{p}{2} & 0 & 0 & 0 \end{pmatrix}, \tag{A.28}$$

where the matrix is block diagonal, with the eigenvalues

$$\lambda_{1,2}(p) = \frac{1}{2}\left(p \pm \sqrt{2p^2 - 2p + 1}\right), \tag{A.29}$$

$$\lambda_{3,4}(p) = \frac{1-p}{2} \geq 0. \tag{A.30}$$

We find that

$$\lambda_1(p) = \frac{1}{2}\left(p - \sqrt{2p^2 - 2p + 1}\right) < 0 \quad \text{for} \quad 0 \leq p < 1, \tag{A.31}$$

meaning that the partial transpose is negative for all $p < 1$ and only becomes positive semidefinite in the trivial limit $p \to 1$. By the PPT criterion $\rho_{AB}(p)$ is

entangled for any nonzero weight of the single-photon component. Combining this with the Wigner function positivity discussed above, one finds that for

$$p \in [1/2, 1)\,, \tag{A.32}$$

the state is simultaneously entangled and Wigner positive, and thus provides a concrete example of *hybrid entanglement* within the $\mathcal{C} \cap \mathcal{Q}$ overlap.

Finally, let us discuss why the beamsplitter transformation preserves the positivity (or negativity) of the Wigner function. A linear-optical transformation, such as the beamsplitter, is generated by a quadratic Hamiltonian and hence corresponds to a Gaussian unitary. Therefore, at the level of canonical operators, it implements a symplectic orthogonal transformation S on the quadrature vectors

$$z_{\text{out}} = S\, z_{\text{in}}, \tag{A.33}$$

making the Wigner function after the beamsplitter

$$W_{\text{out}}(z) = W_{\text{in}}(S^{-1}z), \tag{A.34}$$

thus the beamsplitter does not change the value taken by the Wigner function, but only relabels the phase space coordinates. In our case the Wigner function factorizes as

$$W_{\text{in}} = W_{\rho(p)}(z_1)W_0(z_2), \tag{A.35}$$

with $W_0 \geq 0$ everywhere for the vacuum. The sign of W_{in} is therefore completely determined by $W_{\rho(p)}$. As discussed in the main text $W_{\rho(p)}$ is everywhere nonnegative for $p \geq 1/2$.

B. Gravity–Mediated Entanglement

B.1. GME setup and evolution

The setup used in Kumar et al. [73] is based on a single-particle Gaussian state for both systems A and B in Eq. 4.1 and Eq. 4.2. This two-body state can then be written in terms of a center of mass (COM) wavefunction ϕ and a relative coordinate wavefunction ψ, where the COM coordinate is given by $R = (x_A + x_B)/2$ and the relative coordinate takes the form $r = x_B - x_A$. The initial state of the whole system can then be written as $\Psi(x_A, x_B, 0) = \phi(R, 0)\psi(r, 0)$, where

$$\phi(R,0) = \left(\frac{1}{\pi\sigma^2}\right)^{1/4} \exp\left(-\frac{R^2}{2\sigma^2}\right), \quad \text{and} \tag{B.1}$$

$$\psi(r,0) = \left(\frac{1}{4\pi\sigma^2}\right)^{1/4} \exp\left(-\frac{r^2}{8\sigma^2} - i\frac{p_0}{\hbar}r\right). \tag{B.2}$$

For our purposes it is required to work with density matrices, so the initial density matrix element $\langle x_A, x_B| \rho_0 |y_A, y_B\rangle$ in relative coordinates is given by

$$\rho(R_x, r_x, R_y, r_y, 0) = \frac{1}{2\pi\sigma^2} \exp\left(-\frac{R_x^2 + R_y^2}{2\sigma^2}\right) \exp\left(-\frac{r_x^2 + r_y^2}{8\sigma^2} - i\frac{p_0}{\hbar}(r_x - r_y)\right), \tag{B.3}$$

where R_x/R_y and r_x/r_y are defined as above. Recalling the definitions of the classical von Neumann equation in Eq. 2.24 and the regular von Neumann equation in Eq. 2.31, it is clear that the potential has to be expanded at least to third order (see Eq. (4.8)) to obtain any quantifiable difference between the two evolutions.

To transform these equations to a useful form however, we first have to transform

the derivatives via

$$\partial_{x_A}^2 = \left(\frac{1}{2}\partial_{R_x} - \partial_{r_x}\right)^2, \tag{B.4}$$

$$\partial_{x_B}^2 = \left(\frac{1}{2}\partial_{R_x} + \partial_{r_x}\right)^2, \tag{B.5}$$

$$\partial_{y_A}^2 = \left(\frac{1}{2}\partial_{R_y} - \partial_{r_y}\right)^2, \tag{B.6}$$

$$\partial_{y_B}^2 = \left(\frac{1}{2}\partial_{R_y} + \partial_{r_y}\right)^2, \tag{B.7}$$

making the kinetic part of our Hamiltonian

$$-\frac{\hbar^2}{2m}\left[(\partial_{x_A}^2 + \partial_{x_B}^2) - (\partial_{y_A}^2 + \partial_{y_B}^2)\right] = -\frac{\hbar^2}{2m}\left[\frac{1}{2}\left(\partial_{R_x}^2 - \partial_{R_y}^2\right) + 2\left(\partial_{r_x}^2 - \partial_{r_y}^2\right)\right], \tag{B.8}$$

while the potential takes the simple form

$$V(x_B - x_A) - V(y_B - y_A) = V(r_x) - V(r_y). \tag{B.9}$$

Now since we are only interested in the gravitational interaction between the two test masses and generally neglect the COM motion of the system (as it only undergoes free evolution), we will drop the ϕ part of our state for the remainder of the discussion. This brings us to the final classical von Neumann equation in Eq. (4.4) and the quantum counterpart in Eq. (4.5).

The split step evolution described in section 4.3 to propagate this part of the density matrix is done by the following function in B.1. Note that the grid is centered around the classical trajectory, to avoid boundary errors.

```
def classical_evolution(final_time, dt, L, p0_mL, sigma):
    p0 = p0_mL * m * L
    mu = m/2
    steps = int(np.round(final_time/dt))

    # --- Grid around r_cl(t) \approx -2 p0 t / m ---
    r_cl_final = -2 * p0 * final_time / m
    pad = 30 * sigma
    r_min = min(-5*pad, r_cl_final - 5*pad)
    r_max = max(+5*pad, r_cl_final + 5*pad)

    N = 512
    r_grid = np.linspace(r_min, r_max, N, dtype=float)
    dr = r_grid[1] - r_grid[0]
    rx, ry = np.meshgrid(r_grid, r_grid, indexing='ij')
```

```
    # --- Initial density matrix at r=0, Eq. (5) ---
    gaussian = np.exp(- (rx**2 + ry**2) / (8 * sigma**2))
    phase = np.exp(-1j * p0 * (rx - ry) / hbar)
    rho0 = (1 / np.sqrt(4 * np.pi * sigma**2)) * gaussian * phase
    rho0 = normalize_density_matrix(rho0, dr)
    rho = 0.5 * (rho0 + rho0.conj().T)  # hermitize

    # --- Precompute k-grid and kinetic phase ---
    k = 2 * np.pi * fftfreq(N, d=dr)
    kx, ky = np.meshgrid(k, k, indexing='ij')
    K = (hbar / (2*mu)) * (kx**2 - ky**2)
    kinetic_phase = np.exp(-1j * K * dt)

    print(f"Grid: [{r_min*1e9:.3f}, {r_max*1e9:.3f}] nm, dr={dr*1
    e12:.3f} pm; r_cl(T)={r_cl_final*1e9:.3f} nm")

    # --- Symmetric split-operator with exact V-difference ---
    for step in tqdm(range(steps), desc="Evolution"):
        V_phase_half = np.exp( -1j * V_classical(rx, ry) * (dt/(2*
    hbar)) )
        rho = V_phase_half * rho
        rho = ifft2( kinetic_phase * fft2(rho) )
        rho = V_phase_half * rho

        # ensure hermitian & normalized
        rho = 0.5 * (rho + rho.conj().T)
        if (step+1) % 20 == 0:
            rho = normalize_density_matrix(rho, dr)

    rho = normalize_density_matrix(rho, dr)
    rho = 0.5 * (rho + rho.conj().T)
    return rho, r_grid, dr
```

Listing B.1: Evolution of relative coordinate density matrix.

To then obtain the covariance data from this evolved relative coordinate density matrix, we make use of the derived identities in Eqs. (4.10-4.17), which is done by the following function:

```
def rel_moments_from_rho(rho, r_grid, dr, hbar):
    diag = np.real(np.diag(rho)).astype(np.float64, copy=True)
    Z = float(diag.sum() * dr)
    pdf = diag / Z

    r = r_grid.astype(np.float64, copy=False)
    r_mean = (r * pdf).sum() * dr
    r2_mean = (r * r * pdf).sum() * dr

    N = r.size
```

```
    k = 2 * np.pi * np.fft.fftfreq(N, d=dr)

    # d/dy at diagonal
    rho_fft_y = np.fft.fft(rho, axis=1)
    d_rho_dy = np.fft.ifft((1j * k)[None, :] * rho_fft_y, axis=1)
    d_rho_dy_diag = np.diag(d_rho_dy)

    # d^2/dy^2 at diagonal
    d2_rho_dy2 = np.fft.ifft(-(k**2)[None, :] * rho_fft_y, axis=1)
    d2_rho_dy2_diag = np.diag(d2_rho_dy2)

    p_mean = (-1j * hbar * d_rho_dy_diag.sum() * dr).real
    p2_mean = (-(hbar**2) * d2_rho_dy2_diag.sum() * dr).real

    # d/dx at diagonal (for {r,p})
    rho_fft_x = np.fft.fft(rho, axis=0)
    d_rho_dx = np.fft.ifft((1j * k)[:, None] * rho_fft_x, axis=0)
    d_rho_dx_diag = np.diag(d_rho_dx)

    anticom = (-1j * hbar * (r * (d_rho_dy_diag - d_rho_dx_diag)).
    sum() * dr).real
    cov_rp = 0.5 * anticom - r_mean * p_mean

    var_r = r2_mean - r_mean**2
    var_p = p2_mean - p_mean**2
    return dict(r_mean=r_mean, p_mean=p_mean, var_r=var_r, var_p=
    var_p, cov_rp=cov_rp)

def com_moments(t, m, sigma, hbar):
    omega0 = hbar / (2 * m * sigma**2)
    var_R  = 0.5 * sigma**2 * (1 + (omega0 * t)**2)
    var_P  = hbar**2 / (2 * sigma**2)
    cov_RP = 0.5 * hbar * omega0 * t
    return dict(var_R=var_R, var_P=var_P, cov_RP=cov_RP)

def total_sigma_lab(rel, com):
    var_r, var_p, cov_rp = rel["var_r"], rel["var_p"], rel["cov_rp
    "]
    var_R, var_P, cov_RP = com["var_R"], com["var_P"], com["cov_RP
    "]

    s00 = var_R + 0.25 * var_r
    s02 = var_R - 0.25 * var_r
    s11 = 0.25 * var_P + var_p
    s13 = 0.25 * var_P - var_p
    s01 = 0.5 * cov_RP + 0.5 * cov_rp
    s03 = 0.5 * cov_RP - 0.5 * cov_rp

    Sigma = np.array([
```

```
        [s00, s01, s02, s03],
        [s01, s11, s03, s13],
        [s02, s03, s00, s01],
        [s03, s13, s01, s11],
    ], dtype=float)
    return Sigma
```

Listing B.2: Covariance data from the relative coordinate density matrix.

B.2. Numerical details

B.2.1. Parameters

To obtain the results of Sec. 4.4, the system is propagated forward with $dt = 10^{-5}$ s, up to the final time of 2 s, which represents typical coherence times for experimentally feasible states. The momentum ratio p_0/mL is chosen to be 1, as varying the momentum has only a slight impact on the outcome of the evolution. Finally, the initial spread is set to 1 nm, and the spatial grid is separated into $N = 512$ points along each direction. These parameter choices are then plugged into B.1, to obtain the final classical state, or conversely, the final quantum state by replacing the classical potential term $(x-y)V'\left(\frac{x+y}{2}\right)$, with $V(x)-V(y)$. Naturally, this code can also be extended to periodically save certain parameters like the trace distance of Fig. 4.3.

B.2.2. Robertson–Schrödinger condition

An important first check of the evolution code is to make sure that covariance–based uncertainty relations are never violated for the quantum evolution. These are checked by numerically evaluating $RS = \Sigma + \frac{i\hbar}{2}\Omega$ and checking how much it deviates from 0. In particular, when evolving this setup for 2 s, with $\sigma = 1$ nm, $p_0/mL = 1$ and $N = 512$, we find, for the quantum evolution under third–order truncation, an RS violation (scaled with $\hbar$) of $\mathrm{RS}_{\mathrm{min}} = -4.010 \cdot 10^{-111}$, which is clearly a numerical artifact. Similarly, we also find that the RS violation of the classical evolution, with the same parameters, also truncated at third order, gives a negligible violation of $\mathrm{RS}_{\mathrm{min}} = -3.280 \cdot 10^{-16}$. The RS–condition presents a compelling consistency check, as it is never enforced by hand in the simulation code. The only things that are manually forced every few iteration steps are the normalization and hermiticity to avoid numerical errors. Also note that the RS violation of the classical evolution, while still tiny, is orders of magnitude bigger than the quantum counterpart. This suggests that we do not get representational entanglement for all times, and we conjecture that there exist large enough timescales at which an RS violation of the classically evolved state becomes detectable.

B.2.3. Wigner function

The behaviour of the Wigner function in the quantum evolution at third order is another important check we can make. Especially emerging Wigner negativity in the numerics would highlight some consistency with the short–time analytical results of Sec. 4.4, as well as external numerical results [73]. However, let us first check the basics. The normalization condition is satisfied to very high accuracy, i.e., the same parameters used above give

$$\int dr dp\, W(r,p) \approx 1.00000000, \tag{B.10}$$

which is no surprise, as the density matrix is renormalized every few iteration steps. The integrated absolute value on the other hand gives

$$\int dr dp |W(r,p)| \approx 1.18245104, \tag{B.11}$$

which corresponds to a negativity volume of

$$\int dr dp\, \max(0,-W) \approx 9.122552 \cdot 10^{-2}, \tag{B.12}$$

confirming the emergence of Wigner negativity in this numerical framework. Finally, the Wigner function is plotted in Fig. B.1.

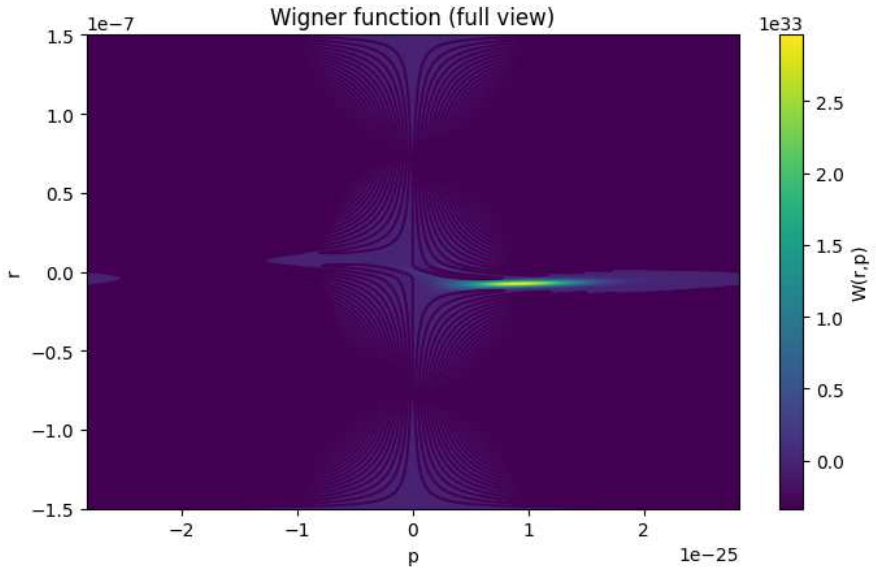

Figure B.1.: Wigner function heatmap of the third–order truncation of the quantum evolution for 2 s, with $\sigma = 1$ nm, $p_0/mL = 1$ and $N = 512$.